Chapter 2
Particle Detectors

Abstract The subject of the second chapter is the interaction of particles with matter. The first section discusses the mechanism by which various types of particles interact with different media. Particular emphasis is given to the concept of energy loss and range in matter. The second section focuses on the experimental techniques for particle identification. The third section is dedicated to the functioning of particle detectors.

2.1 Passage of Particles Through Matter

The kinematics of a particle moving through matter is affected by the interaction with the medium, which can be traced back to one or multiple incoherent collisions with the scattering centres, or to coherent effects that involve the medium as a whole. When the interaction is elastic, the particle transfers to the medium part of its energy or momentum at each collision. This is the case of the energy loss by electron collision, multiple scattering, Compton scattering. Inelastic reactions absorb or transmute the particle into something else, and can also give rise to new forms of radiation or leave behind excited states. This is for example the case of photon conversion, bremsstrahlung, neutron capture, charged-current neutrino interactions. Depending on the particle type, on its energy, and on the properties of the medium, one mechanism usually dominates over the others.

Energy Loss by Collision

Moderately relativistic charged particles lose energy mostly by the interaction with the electromagnetic field of atoms (electron collision). In the $10^{-1} \lesssim \beta\gamma \lesssim 10^3$ regime, the rate of energy loss per unit of traversed length, dE/dx, depends almost exclusively on the particle velocity β and on the properties of the medium. The formula describing the average rate of energy loss, or *linear stopping power*, is called *Bethe formula* and is given by:

$$-\frac{dE}{dx} = 2\pi\, N_{\mathrm{A}}\, \rho\, \frac{Z}{A}\, \frac{\alpha^2(\hbar c)^2}{m_e\, c^2}\, \frac{z^2}{\beta^2} \left[\ln \frac{2\, m_e\, c^2\, \gamma^2\, \beta^2\, W_{\max}}{I^2} - \beta^2 - \delta(\beta) - 2\frac{C(I,\beta)}{Z} \right], \quad (2.1)$$

L. Bianchini, *Selected Exercises in Particle and Nuclear Physics*,
UNITEXT for Physics, https://doi.org/10.1007/978-3-319-70494-4_2

with:

N_A, α	Avogadro number (6.02×10^{23} mol^{-1}) and fine structure constant ($\alpha \approx 1/137$)
ρ, A, Z	mass density (g cm^{-3}), atomic weight (g mol^{-1}), and atomic number of the material
z, β, γ	electric charge in units of e, velocity, and gamma-factor of the incident particle
W_{max}	maximum energy transfer in a binary collision (see Problem 1.26 for its derivation)
I	mean excitation potential of the material, given by the approximate formula $I \approx 16 \cdot Z^{0.9}$ eV.
δ, C	*density* and *shell* corrections factors, see Problem 2.2. For their parametrisation, the reader is addressed to more advanced textbooks on the topic.

The units of dE/dx deserve a few more words. It is quite common to express the energy loss as a *mass stopping power*, i.e. in units of MeV g^{-1} cm^2 rather than in MeV cm^{-1}. This is motivated by the fact that the energy loss by collision is proportional to the density of scattering centers, i.e. $Z\, N_A\, \rho/A$. Since Z/A is quite uniform across different materials, the energy loss per unit of surphace density is less dependent on the medium.

As shown by Eq. (2.1), for a fixed medium the energy loss by collision depends only on the particle velocity β and on its charge z. The functional form features a fast rise as β approaches 0 due to the β^{-2} factor, it approaches a global minimum at around $\beta \approx 0.94 \div 0.97$, or γ between about 3 and 4, and then rises logarithmically with γ. Particle sitting on the minimum and on the plateau of their dE/dx curve are characterised by a rather uniform and close-to-minal energy loss, and for this reason they are said to be minimum ionising particles (MIP). Using the approximation $m_e/M \ll 1$ in Eq. (1.141) for the maximum energy transfer, and neglecting both shell and density corrections, which are however relevant for large γ, we can arrive an approximate formula:

$$-\frac{dE}{dx} \approx \left(0.307 \text{ MeV mol}^{-1} \text{ cm}^2\right) \rho \frac{Z}{A} \frac{z^2}{\beta^2} \left[\ln \frac{2\, m_e\, c^2\, \gamma^2\, \beta^2}{I} - \beta^2\right]. \tag{2.2}$$

Considering that for most of the elements and their compounds $Z/A \approx 0.5$ g^{-1} mol, and given that the term within square brackets is slowly varying with γ between 10 and 15, when dealing with particles of sufficiently large initial energy, one can often use an average value:

$$-\frac{dE}{dx} \approx 1.5 \div 2.0 \left(\frac{\rho}{\text{g cm}^{-3}}\right) \frac{z^2}{\beta^2} \text{ MeV/cm}. \tag{2.3}$$

Figure 2.1 shows the function at the right-hand side of Eq. (2.2) for $Z/A = 0.5$ g^{-1} mol and for two extreme values of the ionisation potential I. The num-

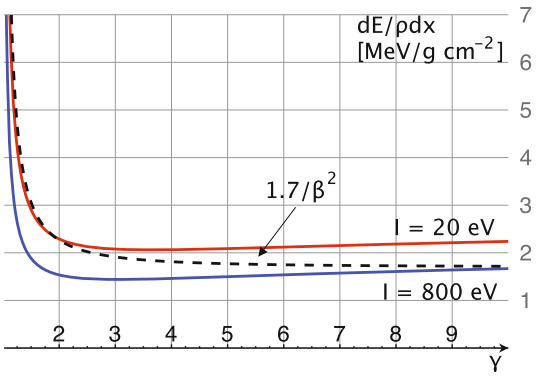

Fig. 2.1 The approximate Bethe formula of Eq. (2.2) as a function of the γ factor of the incident particle and for two extreme values of the mean excitation potential I. The global minimum at around $\gamma = 3 \div 4$ and the logarithmic growth are evident from the curves. For values of γ above the argmin of the function, the mass stopping power is in the ballpark of 2 MeV g^{-1} cm^2

ber of electrons extracted from their orbitals per unit length by the interaction with a MIP can be crudely estimated from Eq. (2.3) to be

$$\frac{dN_e}{dx} \approx \frac{1}{I}\frac{dE}{dx}. \tag{2.4}$$

For example, for a typical ionisation potential $I = 20$ eV and a water-like mass density, a unit-charge MIP produces about 10^5 electrons/cm.

For electrons and positrons moving inside matter, a formula similar to Eq. (2.1) holds. A few modifications have to be introduced, however, to account for the smaller mass and for the identity of the incident electron with the electrons that it ionizes, see e.g. Sect. 2.4 of Ref. [1] or Sect. 33.4 of Ref. [2]. In particular, one needs to replace $W_{\max}$ by $m_e c^2(\gamma - 2)/2$ and $2\, m_e c^2$ by $m_e c^2$ in the argument of the logarithm, and add a number of extra β-dependent terms inside the square brackets of Eq. (2.1), giving:

$$-\frac{dE}{dx} = \frac{(0.307 \text{ MeV mol}^{-1} \text{ cm}^2)}{2}\rho\frac{Z}{A}\frac{z^2}{\beta^2}\times$$
$$\times\left[\ln\frac{m_e c^2 \gamma^2 \beta^2 (m_e c^2(\gamma-1))}{2I^2} + \frac{1}{\gamma^2} - \frac{2\gamma-1}{\gamma^2}\ln 2 + \frac{1}{8}\left(\frac{\gamma-1}{\gamma}\right)^2 - \delta(\beta)\right] \tag{2.5}$$

Numerically, it turns out that the stopping power for heavy ions and electrons and positrons with the same velocity β are rather similar, indeed they are consistent with each other to within about 15% up to γ factors of about 100, after which energy loss by radiation prevails anyway. The relative difference between Eqs. (2.1) and (2.8) for a few illustrative values of γ is reported in Table 2.1.

Table 2.1 Relative difference between the energy loss by collision dE/dx for ions and electrons at the same velocity and for a value of the mean excitation potential $I = 20$ (800) eV. The density correction δ is neglected

γ	β	$\frac{dE_{\text{ion}}/dx - dE_e/dx}{dE_{\text{ion}}/dx}$
1.01	0.140	11.3% (17.1%)
1.1	0.417	10.7% (16.3%)
2	0.866	8.48% (12.5%)
4	0.968	8.10% (11.4%)
10	0.995	9.06% (12.2%)
100	0.999	12.3% (17.5%)

The ionisation charge and the residual atomic excitation produced by the passage of a charged particle can be detected through various methods and thus yield a measurement of the particle position or energy. For example, this is the working principle of gaseous detectors like proportional chambers, drift and streamer tubes, RPC, liquid noble-gas detectors, etc. Semiconductor materials are also largely employed in experiments. When a charged particle moves inside a semiconductor, a number of electron-hole pairs are produced by the electrons being excited from the valence to the conductive band. One strength of these materials relies on their small band gap energy, a few eV infact, yielding a large number of signal carriers. Through appropriate doping and polarisation of the semiconductor, these electron-hole pairs can drift across the medium without significant recombination, to be finally collected for signal generation.

Other materials have the property of converting a fraction of the energy lost by a moving charged particle in the form of molecular or electronic excitation of long-lived states, that subsequently decay by emitting photons of characteristic wavelength (fluorescence). Because of such property, these materials are called *scintillators*, and the emitted radiation is called *scintillation light*. A key property of the scintillation mechanism is that the medium is transparent to its own light over distances large enough that the photons can be efficiently collected. The total light output per unit length is approximately proportional to the stopping power, a property which can also allow one to measure the total particle energy for fully absorbed particles. Scintillators can be classified into two families: *organic*, for which the scintillation mechanism relies on the fluorescence of organic molecules (e.g. plastic, organic crystals), and *inorganic*, for which the fluorescence originates from the band structure of the crystal (possibly activated by the introduction of suitable inpurities), or from electron-ion or ion-ion recombination. A broader overview on the field can be found in e.g. Chap. 7 of Ref. [1].

Table 2.2 shows the mean energy loss necessary to produce one signal carrier, which can be either a ion-electron pair, an electron-hole pair, or a scintillation photon, depending on the excitation mechanism. As shown in the table, the largest signal yields are provided by semiconductors, followed by the best scintillators and by ionisation in noble gases. Some of the most popular scintillators materials in HEP are actually characterised by relatively low light yield.

Table 2.2 Mean energy loss necessary to produce one signal carrier, listed in increasing order. For scintillators, the mean energy is defined as the inverse of the light yield (LY) in [γ/MeV], a quantity that is commonly used to quantify the brightness of the scintillator. The values are taken from Ref. [1, 2] and, since they usually depend on the ambiental conditions, they should be considered more as an order-of-magnitude estimate. For more precise values, the reader is addressed to the technical literature

Material	Excitation	Mean excitation energy ε [eV]
Ge (77 K)	Electron-hole	3.0
Si	Electron-hole	3.6
Cs I (Tl)	Scintill. γ	12
Na I (Tl)	Scintill. γ	22
Xe	Electron-ion	22
Isobutane	Ionisation	23
Ar	Electron-ion	26
CO_2	Ionisation	33
LISO (Ce)	Scintill. γ	35
He	Electron-ion	41
Plastic	Scintill. γ	100
BGO	Scintill. γ	300
PbWO	Scintill. γ	5000

Multiple Scattering

Multiple scattering (MS) through small angles refers to the ensemble of incoherent elastic collisions against the nuclear fields that charged particles undergo when crossing a piece of material. Their collective effect it to randomise the direction of the incoming particle with no significant energy loss. More informations on the subject can be found in Ref. [2]. The probability of multiple scattering through small angles is large because of the $\sin^{-4}\theta/2$ dependence of the Rutherford cross section (see Problem 1.58). However, there is also some finite probability that the scattering occurs at large angles, with subsequent emission of a knocked-out electron, or δ-ray (see Problem 1.62 for how to estimate such a probability). The quantity that characterises multiple scattering through small angles is the mean square angle per unit length Θ_s^2, which in the standard theory is given by:

$$\Theta_s^2 = \left(\frac{E_s}{\beta c|\mathbf{p}|}\right)^2 \frac{1}{X_0}, \quad \text{with} \quad E_s = \sqrt{\frac{4\pi}{\alpha}} m_e c^2 = 21 \text{ MeV}. \tag{2.6}$$

Notice that the quantity E_s is the same that enters the definition of the *Molier radius* for the lateral width of an electromagnetic shower, see Problem 2.34. The effect of MS inside a medium of length L and radiation length X_0 is to randomise the position and direction of a charged particle at the exit of the medium. Considering their projections onto a plane, the displacement y and angle θ_y are described by the joint p.d.f:

$$p(y, \theta_y \mid L) = \frac{2\sqrt{3}}{\pi} \frac{1}{\Theta_s^2 L^2} \exp\left[-\frac{4}{\Theta_s^2} \left(\theta_y^2 - \frac{3\, y\, \theta_y}{L} + \frac{3\, y^2}{L^2} \right) \right] \tag{2.7}$$

From Eq. (2.7), one can easily compute the standard deviation of θ_y and y, and their correlation:

$$\sqrt{\langle \theta_y^2 \rangle} = z \sqrt{\frac{\Theta_s^2 L}{2}} = z \frac{14.8\ \text{MeV}}{\beta c |\mathbf{p}|} \sqrt{\frac{L}{X_0}} \tag{2.8}$$

$$\sqrt{\langle y^2 \rangle} = \sqrt{\langle \theta_y^2 \rangle} \frac{L}{\sqrt{3}} = z \frac{8.54\ \text{MeV}}{\beta c |\mathbf{p}|} \sqrt{\frac{L}{X_0}}\, L$$

$$\frac{\langle y\, \theta_y \rangle}{\sqrt{\langle \theta_y^2 \rangle \langle y^2 \rangle}} = \frac{\sqrt{3}}{2}. \tag{2.9}$$

A more accurate treatment of MS modifies the first of Eq. (2.8) to the well-known formula:

$$\sqrt{\langle \theta_y^2 \rangle} = z \frac{0.0136\ \text{GeV}}{\beta c |\mathbf{p}|} \sqrt{\frac{L}{X_0}} \left[1 + 0.038\, \ln\left(\frac{L}{X_0} \right) \right], \tag{2.10}$$

See Ref. [2] for further informations.

Energy Loss by Bremstrahlung

For energies above a material-dependent threshold known as *critical energy* (E_c), energy loss by radiation in the electromagnetic field of the atoms (*bremsstrahlung*) prevails. An approximate parametrisation for the critical energy for electrons and positrons is provided by the formula

$$E_c = \frac{800\ \text{MeV}}{(Z + 1.2)}. \tag{2.11}$$

In the bremsstrahlung-dominated regime, the energy loss per unit length is approximately proportional to the energy itself:

$$-\frac{dE}{dx} = \frac{E}{X_0}, \tag{2.12}$$

where X_0, called *radiation length*, is approximately independent of E. In units of mass per unit area, the radiation length is provided by the approximate expression:

$$\begin{aligned} X_0 &= \frac{(m_e\, c^2)^2 A}{4\, Z\, (Z + 1)\, N_A\, \alpha^3 (\hbar c)^2 \left[\ln(183 Z^{-1/3}) - f(Z) \right]} \\ &\approx \frac{716\, A\ \text{g cm}^{-2}}{Z(Z + 1) \ln(287\sqrt{Z})} \approx 180 \frac{A}{Z^2}\ \text{g cm}^{-2}, \end{aligned} \tag{2.13}$$

Table 2.3 Radiation lengths for some materials that can be commonly found in particle physics experiments, listed by decreasing order or X_0 [cm]. From Ref. [1]

Material	X_0 [g/cm^2]	X_0 [cm]
Air	36	300×10^2
Scintill.	44	42
H_2O	36	36
Si	21.9	9.4
NaI	9.5	2.6
Fe	13.8	1.8
BGO	8.0	1.1
Pb	6.4	0.56

where A is the mass number in units of g mol^{-1}. More informations on $f(Z)$ can be found in dedicated textbook, see e.g. Ref. [1]. Notice that both the nucleus and the atomic electrons contribute to this $\mathcal{O}(\alpha^3)$ process: the former through a charge $Z\,e$ (hence the term $\sim Z^2$), the latter through Z incoherent scatterings of strength e (hence the term $\sim Z$). The last of Eq. (2.13) is a further approximation that helps remembering the order-of-magnitude of X_0 and its dependence on the atomic and mass number. The radiation length for a few representative materials commonly found in particle physics experiments are reported in Table 2.3. The energy loss by radiation is the dominant mechanism of energy degradation for ultra-relativistic charged particles. Notice that the radiation length X_0 is proportional to the mass squared of the charged ion (m_e in Eq. (2.13)). The next-to-lightest charged particle is the muon with a mass nearly 200 times larger than m_e. The threshold at which energy loss by radiation starts to be comparable to energy loss by collision is therefore much higher.

Energy Loss by Coherent Radiation: Cherenkov and Transition Radiation

If $\beta > 1/n(\omega)$, $n(\omega)$ being the refraction index of the medium at the frequency ω, the particle emits energy in the form of *Cherenkov radiation* of wavelength $\lambda = 2\pi\, c/\omega$. The energy loss per unit length is given by:

$$-\frac{dE}{dx} = z^2 \frac{\alpha\,\hbar}{c} \int d\omega\, \omega \sin^2 \theta_c(\omega), \tag{2.14}$$

where θ_c is the angle of the shock-wave direction with respect to the particle direction, which satisfies the relation:

$$\cos\theta_c = \frac{1}{\beta\, n}. \tag{2.15}$$

Although the Cherenkov spectrum is continuous, photodetectors have a limited range of sensitivity which depends of the quantum efficiency of the photocathode. In order to estimate the number of photons to which the detector will be sensitive, we can integrate Eq. (2.13) over the relevant spectrum to yield:

$$\frac{dN_\gamma}{dx\,d\lambda} = \frac{2\pi\,\alpha\,z^2}{\lambda^2}\sin^2\theta_c(\lambda) \quad \Rightarrow \quad \frac{dN_\gamma}{dx} \approx 2\pi\alpha z^2\,\langle\sin^2\theta_c\rangle\,\frac{\lambda_2-\lambda_1}{\lambda_1\lambda_2} \tag{2.16}$$

$$\frac{N_\gamma}{L} \approx \frac{1.15\times10^3}{(\hat{\lambda}/400\text{ nm})}z^2\,\langle\sin^2\theta_c\rangle\,\frac{\Delta\lambda}{\hat{\lambda}}, \tag{2.17}$$

where $\hat{\lambda} = \sqrt{\lambda_1\lambda_2}$ and the mean value of $\sin^2\theta_c$ is used, which is appropriate if n is slowing varying. For example, with a photodetector sensitive in the range 300 to 500 nm, this gives $N_\gamma \lesssim 500$ photons/cm for a particle with $z = 1$, to be compared with the about 10^5 electrons/cm electrons released by a MIP from collision loss, see Eq. (2.7). When coupled to a photodetector, the geometric and quantum efficiency of the photocathode further reduce the photo-electrons (p.e.) output. Equation 2.16 for $z = 1$ can be written as:

$$N_{\text{p.e.}} = L\,N_0\,\langle\sin^2\theta_c\rangle \tag{2.18}$$

where N_0 is the so-called *Cherenkov detector quality factor*, which is of order 100 cm^{-1} for realistic photodetectors sensitive in the visible-UV range: practical counters in experiments feature values of the quality factor ranging between 30 and 180 cm^{-1} [2].

Detectors based on the detection of Cherenkov radiation can be used for measuring the total energy of the crossing particle as well as for particle identification. In the first case, one exploits the proportionality between the collected light yield and the range of the particle, which is approximately proportional to the initial particle energy, see Problem 2.3. For the second purpose, one should distinguish between *threshold* detectors, which trigger the passage of a particle with velocity above the Cherenkov threshold, and *imaging* detectors, which are instead designed to exploit the angle of emission of individual Cherenkov photons. For highly energetic particles with $\beta \approx 1$, the employment of threshold Cherenkov detectors for particle identification becomes problematic since the index of refraction needs to approach one. To this purpose, radiators with very low density, like He, $C\,O_2$, or silica aerogel, are commonly used. Indeed, the refraction index for a homogeneous medium depends on the density according to the relation:

$$n = 1 + \frac{2\pi\,f(0,\mathbf{k})}{|\mathbf{k}|^2}N, \tag{2.19}$$

where N is the density of scattering centres, $f(0,\mathbf{k})$ is the forward scattering amplitude and $\mathbf{k}$ is the wave-number vector. For example, a simple model based on a collection of damped electronic oscillators with resonant frequency ω_k and damping constant ν_k would give [3]:

$$n(\omega) = 1 + 2\pi\,r_e\,c^2\,N\sum_k \frac{f_k}{\omega_k^2-\omega^2-i\,\nu_k\omega}. \tag{2.20}$$

Table 2.4 Refraction index and γ threshold for various radiators commonly used in Cherenkov detectors. The values refer to wavelengths in the visible domain

Material	$n-1$	γ
He (NTP)	3.3×10^{-5}	123
Air (NTP)	2.7×10^{-4}	43
CO_2 (NTP)	4.3×10^{-4}	34
$C_5\,H_{12}$ (NTP)	1.7×10^{-3}	17.2
Silica aerogel	$0.007 \div 0.13$	$2.1 \div 8.5$
H_2O	0.33	1.52
Glass	$0.46 \div 0.75$	$1.22 \div 1.37$

See Tables 2.4 and 6.1 of Ref. [2] for the index of refraction of some popular radiators. In the $\beta \to 1$ regime, though, the light output becomes small as for Eq. (2.16). For example, if a threshold Cherenkov is used for particle identification in a beam of fixed momentum $\mathbf{p}$, the refraction index can be set to the inverse velocity of the slowest particle, say β_2, and then:

$$\langle \sin^2 \theta_c \rangle = 1 - \frac{\beta_2^2}{\beta_1^2} = \frac{1 - m_1^2/|\mathbf{p}|^2 - 1 + m_2^2/|\mathbf{p}|^2}{\beta_1^2} = \frac{m_2^2 - m_1^2}{|\mathbf{p}|^2 + m_1^2}, \tag{2.21}$$

which decreases like the square of the beam momentum.

When a relativistic charged particle crosses the boundary between vacuum and a medium, a coherent radiation is emitted in the forward region $\theta \sim 1/\gamma$. The total energy radiated depends linearly on the γ factor of the particle according to the formula:

$$I = \alpha\, z^2\, \gamma\, \frac{\hbar\, \omega_p}{3} = \left(0.07\, z^2 \sqrt{\frac{\rho}{\mathrm{g\ cm^{-3}}} \frac{Z}{A}}\ \mathrm{eV} \right) \gamma, \tag{2.22}$$

where $\omega_p = \sqrt{4\pi\, n_e/m}\, e$ is the *plasma frequency* of the medium [3]. Although the energy emitted per each crossing is rather small, the total yield for particles with large γ, like GeV-electrons can be enhanced by interleaving several layers of medium, as it is usually done in the so-called *transition radiation detectors* (TRD). The latter find applications as tracking devices with built-in particle-identification capability. In terms of emitted photons, the spectrum is concentrated in the region $0.1\,\gamma < \omega/\omega_p < \gamma$, so that more energetic particles give rise to a harder spectrum. More informations on the subject can be found in Ref. [2].

Interaction of Photons with Matter

Photons interact with matter by three mechanisms: *photoelectric effect*, *Rayleigh and Compton scattering*, and *pair-production*. Depending on the material and on the photon energy, one mechanism at the time usually dominates over the others. The

photoelectric effect consists in the absorption of the photon by an atom, with the subsequent expulsion of an electron of energy

$$E_e = h\nu - \mathscr{B}_e, \tag{2.23}$$

where $h\nu$ is the photon energy and $\mathscr{B}_e$ is the electron binding energy. Conversely, photon scattering against the atomic electrons does not destroy the photon, but modifies its energy and direction, see e.g. Problem 1.25. The scattering can either leave the atom in the ground state (coherent, or Rayleigh scattering) or kick-out the electron (incoherent, or Compton scattering), thus leaving the atom in an excited state. Pair-production is the conversion of a photon into e^+e^- in the electromagnetic field of the atom, see e.g. Problem 1.48 for the kinematics of this reaction.

At low energy, photoelectric effect prevails. As the atomic electrons are bound in discrete states, the photoelectric cross section as a function of the photon energy features a number of thresholds corresponding to the opening of new atomic level. For energies above the innermost level, the so-called K-shell, the cross section steeply falls with energy like $\sim E^{7/2}$. The K-shell threshold for high-Z elements can be crudely estimated by using the energy levels formula for the hydrogen atom:

$$E(n) = -\frac{1}{2\,n^2}\alpha^2\,Z^2\,m_e\,c^2. \tag{2.24}$$

From this approximations, one expects $E_K \approx 10$ keV for metals like iron (measured value 7.1 keV), and $E_K \approx 100$ keV for lead (measured value 88 keV). At lower energies, the L and M atomic levels give rise to as many new thresholds. Depending on the photon energy, the cross section changes with the atomic number of the medium. For MeV photons, it is roughly proportional to Z^β, with $\beta = 4 \div 5$. The cross section at the K-threshold is of the order of 10^3 barn in lead and about 10^6 barn in iron. See Ref. [9] for a compendium of measured values.

Above the K-threshold, the photoelectric and Compton scattering cross sections become of comparable size. The latter changes mildly with energy for photon energies up to the pair-production threshold, after which pair-production becomes dominant. For $k \equiv E/m_e \lesssim 2$, the total cross sections is approximately given by the *Klein–Nishina formula* for Z incoherent scattering centers [9]:

$$\sigma_{\text{Comp}} = Z\,\sigma_{\text{KN}} \approx Z\left(\frac{8\pi}{3}r_e^2\right)\frac{1+2\,k+1.2\,k^2}{(1+2\,k)^2} \tag{2.25}$$

with $8\pi/3r_e^2 = 0.665$ barn. The low-energy limit of Eq. (2.25) gives the *Thomas cross section* for Z free electrons, while the k-dependent term reduces the cross section for increasing photon energies. In the Compton scattering, a fraction of the photon energy is transferred to the outgoing electron. The differential cross section in the recoil energy of th electron T can be obtained from the Klein–Nishina formula, giving

$$\frac{d\sigma_{\text{Comp}}}{dT} = \frac{3\,\sigma_{\text{Th}}}{8\,m_e\,c^2\,k^2}\left[2 + \frac{\left(\frac{T}{E}\right)^2}{k^2\left(1-\frac{T}{E}\right)^2} + \frac{\frac{T}{E}}{1-\frac{T}{E}}\left(\frac{T}{E} - \frac{2}{k}\right)\right] \qquad (2.26)$$

$$\text{with} \quad 0 \le T \le \frac{2\,k}{1-2\,k}E,$$

see also Problem 1.25. Due to the second term within square brackets in Eq. (2.26), the differential cross section rises steeply with T up to the kinetic bound, giving rise to a characteristic peak in the electron spectrum known as *Compton peak*.

When the photon energy exceeds the e^+e^- threshold, pair-production in the nuclear and electronic fields dominates. For energies below about 10 MeV, the interaction cross section varies logarithmically with the photon energy, and then becomes almost independent of energy. Using Tsai's formula [4], we get

$$\frac{d\sigma_{\text{pair}}}{dx} = \frac{A}{X_0\,N_{\text{A}}}\left[1 - \frac{4}{3}x\,(1-x)\right] \quad \Rightarrow \quad \sigma_{\text{pair}} = \frac{7}{9}\frac{A}{X_0\,N_{\text{A}}} \approx 7.2\,Z^2\ \text{mbarn}, \qquad (2.27)$$

where x is the photon energy fraction transferred to the electron/positron, and we have used the last formula in Eq. (2.13) to approximate X_0. Notice that the appearance of macroscopic properties of the medium in the cross section, like the mass number and the Avogadro number, are fictitious, since they exactly cancel the same quantities inside X_0. The latter is conveniently introduced to show that the interaction length for e^+e^- production is indeed related to the radiation length by $\lambda_{\text{pair}} = (9/7)\,X_0$. See Ref. [2] for more details.

Neutrons

The interaction between neutrons and matter depends strongly on the neutron energy. For energies in excess of about 100 MeV, neutrons initiate a hadronic cascade, with the production of primary hadrons (e.g. pions) sharing a fair fraction of the initial neutron energy. *Fast* neutrons, i.e. from a few hundreds of keV to a few tens of MeV, slowly thermalise by elastic scattering in high-Z materials, or faster in hydrogenised materials, see Problem 1.24. Inelastic scattering, like $A(n, n')B$, $A(n, 2n')B$, can also occur in the presence of nuclear resonances. *Epithermal* neutrons, i.e. from about 0.1 eV to about 100 keV, and *thermal* neutrons, i.e. around 25 meV, undergo preferentially nuclear reactions, like radiative neutron capture $A(n, \gamma)B$, nuclear spallation $A(n, p)B$, $A(n, \alpha)B$, and nuclear fission.

Problems

Bando n. 13153/2009

Problem 2.1 Give a qualitative description of how the energy loss by ionisation of a charged particle of mass m depends on the particle momentum.

Solution

The energy loss by ionisation dE/dx of a particle of mass m and charge $z\,e$ is described by the Bethe formula of Eq. (2.1). To good approximation, it is a function of the particle velocity and charge only, namely:

$$-\frac{dE}{dx} = z^2\, f(\beta) = z^2 f'\,(|\mathbf{p}|) \tag{2.28}$$

see also Problem 2.4. At a given value of m, the function $f'(|\mathbf{p}|)$ features the following qualitative behaviour:

$$f'(|\mathbf{p}|) \sim \begin{cases} a\,|\mathbf{p}|^{-2} \ln|\mathbf{p}| & |\mathbf{p}| \gtrsim (m/m_e)\; I \\ b\,|\mathbf{p}|^{-2} + c & |\mathbf{p}| \lesssim m \\ c & |\mathbf{p}| \approx 3m \div 4m \\ c + d\,\ln|\mathbf{p}| & |\mathbf{p}| \gg m \end{cases} \tag{2.29}$$

In words: it first decreases as $|\mathbf{p}|^{-2} \ln|\mathbf{p}|$ at small momenta, until the momentum reaches a few times the mass value. At this point, it plateaus and increases only logarithmically with $|\mathbf{p}|$, see Fig. 2.2.

Bando n. 5N/R3/TEC/2005

Problem 2.2 Motivate the presence of the density and shell correction terms to the Bethe formula.

Discussion

The Bethe formula describes the energy loss of a charged particle due to the elastic collisions with the atomic electrons. In this respect, it assumes that the electrons are at rest compared to the moving particle, which is nearly unaffected by each

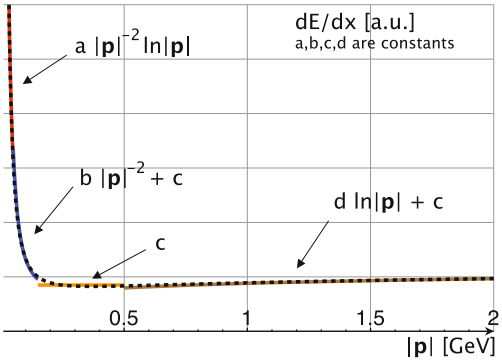

Fig. 2.2 The Bethe formula dE/dx in arbitrary units (a.u.) as a function of $|\mathbf{p}|$, compared to its piecewise approximation in four momentum ranges

individual binary collision. A non-relativistic version of the Bethe-Bloch equation can be indeed obtained by considering the total momentum transfer that an infinitely massive moving charge has on a free electron initially at rest and located at an impact parameter b with respect to the direction of flight. The net effect is obtained by considering an ensemble of such electrons up to a maximum value of b such that the momentum transfer is above the mean ionisation energy necessary to strip the electron from its orbital. See e.g. Sect. 2.2 of Ref. [1].

Solution

The Bethe formula turns out to be accurate in the high- and low-velocity regimes only if the density δ and shell C corrections are added, as shown in Eq. (2.1). The former accounts for the polarisation of the medium by the electric field of the incident particle, which decreases the effective volume available for electron collision. As such, it tends to reduce the energy loss, and is more relevant at high-energy, see e.g. Ref. [2] for a parametrisation of δ. Conversely, if the particle velocity is comparable with the electron velocity, which is of order α, then the assumption that the electrons are at rest breaks down and a correction $C(I, \beta)$ has to be included.

Suggested Readings

The reader is addressed to Sect. 2.2 of Ref. [1] and Chap. 33 of Ref. [2] for further details on this topic.

Problem 2.3 Derive an approximate expression for the range R of a charged particle of mass m and initial energy E that loses energy by collision with the atomic electrons. How does R depends on the initial kinetic energy in the ultra-relativistic limit $E \gg m$ and in the classical limit?

Solution

The energy loss by collision is given by the Bethe formula of Eq. (2.1). The *range* of a particle is the average distance it travels before losing all of its kinetic energy and thus come to a stop. In the *continuous slowing-down approximation* (CSDA), it can be obtained by integrating the inverse linear stopping power over the full range of kinetic energy, i.e.:

$$R(E) = \int_E^m dE \, \frac{1}{dE/dx}. \tag{2.30}$$

The analytical integration of the Bethe formula is an hard task to due to the logarithmic term. However, as we have seen in the introduction Sect. 2.1, for sufficiently large initial energy, one can neglect the dependence of this term on the velocity β and use an approximate version of the type:

$$\frac{dE}{dx} = -\frac{C\, z^2}{\beta^2}, \tag{2.31}$$

with $C \approx 1.7\ \text{MeV}\left[\rho/(\text{g cm}^{-3})\right]\ \text{cm}^{-1}$, see Eq. (2.3). Using Eq. (2.31) in place of the full Bethe formula, the range is given by:

$$R(E) = \int_m^E dE\,\frac{\beta^2}{Cz^2} = \frac{1}{Cz^2}\int_m^E dE\,\left(1-\frac{m^2}{E^2}\right) = \\ = \frac{1}{C\,z^2}\left[(E-m)+m^2\left(\frac{1}{E}-\frac{1}{m}\right)\right] = \frac{1}{C\,z^2}\,\frac{(E-m)^2}{E} = \frac{m}{C\,z^2}\,\frac{(\gamma-1)^2}{\gamma}. \tag{2.32}$$

Hence, we find that R/m is a function of $\gamma = E/m$:

$$\frac{R}{m} = \frac{1}{C\,z^2}\,\frac{(\gamma-1)^2}{\gamma} = \frac{1}{C\,z^2}\,\frac{\left(\sqrt{1+(\beta\gamma)^2}-1\right)^2}{\sqrt{1+(\beta\gamma)^2}}. \tag{2.33}$$

The second of Eq. (2.33) can be directly compared to Fig. 2.3, which shows the range of a heavy ion in different materials as obtained from a full integration of Eq. (2.1), as a function of $\beta\gamma$ (from Ref. [2]). A good numerical agreement is found with the approximate formula of Eq. (2.33) up to $\beta\gamma \gtrsim 1$. For smaller values of β, Eq. (2.33) underestimates the true range by a fair amount. This is a consequence of having neglected the logarithmic term in the stopping power.

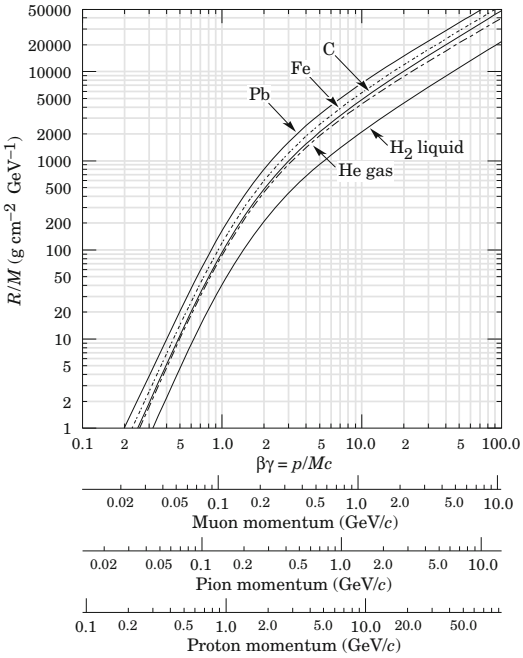

Fig. 2.3 Range of heavy charged particles in liquid (bubble chamber) hydrogen, helium gas, carbon, iron, and lead. From Ref. [2]

According to Eq. (2.32), the range for an ultra-relativistic particle is proportional to its energy:

$$R_{\gamma \gg 1} \approx \frac{m\,\gamma}{C\,z^2} = \frac{E}{C\,z^2}. \tag{2.34}$$

This result comes out intuitive if one considers that a particle with $\gamma \gg 1$ moves at the speed of light; the energy loss is approximately constant until the velocity drops below c. At this point, the stopping power steepens due to the β^{-2} dependence and the residual energy gets degraded in a short path, so that $R \sim E/(dE/dx|_{\text{MIP}}) \sim E$. For a non-relativistic particle, the range is instead a quadratic function of the kinetic energy T:

$$R_{\text{NR}} \approx \frac{(E-m)^2}{C\,z^2\,m} = \frac{T^2}{C\,z^2\,m}. \tag{2.35}$$

However, one should remember that for $\beta \lesssim 0.5$, the approximation of Eq. (2.31) is not valid anymore and the resulting range is underestimated. For example, for an α particle emitted in the decay of ^{210}Po with $T = 5.3$ MeV, the range in air predicted by Eq. (2.35) is about $5.3^2/(2 \cdot 10^{-3} \cdot 2^2 \cdot 4 \times 10^3) \approx 1$ cm, whereas the CSDA range from a full integration of the Bethe function gives about 5 cm [5].

Suggested Readings

A good starting point to learn more about the concept of range is Chap. 2 of Ref. [1].

Problem 2.4 Determine the relation between the stopping power dE/dx for two particles of masses m_1 and m_2, electric charges $z_1\,e$ and $z_2\,e$, and same momentum $|\mathbf{p}|$, moving through the same medium. What is the relation between the range R_1 and R_2 of the two particles under the same conditions?

Solution

The energy loss by collision is given by the Bethe formula of Eq. (2.1), which, as a function of the particle momentum, can be written as:

$$\frac{dE_i}{dx}\,(|\mathbf{p}|) = z_i^2\,f\left(\frac{|\mathbf{p}|}{m_i}\right), \tag{2.36}$$

so that:

$$\begin{aligned}\frac{dE_2}{dx}\,(|\mathbf{p}|) &= z_2^2\,f\left(\frac{|\mathbf{p}|}{m_2}\right) = \frac{z_2^2}{z_1^2}\,z_1^2\,f\left(\frac{m_1}{m_2}\frac{|\mathbf{p}|}{m_1}\right) \\ &= \frac{z_2^2}{z_1^2}\frac{dE_1}{dx}\left(\frac{m_1}{m_2}|\mathbf{p}|\right).\end{aligned} \tag{2.37}$$

Owing to such scaling law, the stopping power $dE(|\mathbf{p}|)/dx$ as a function of $|\mathbf{p}|$ for different particle types are all related by a uniform scaling of the orizontal axis equal the mass ratio, and by a scaling on the vertical axis by the ratio of the squared charges.

Let's now consider the range as defined in Problem 2.3. For a given kinetic energy T, the range is given by:

$$R_i(T) = \int_T^0 dE \, \frac{1}{dE_i/dx} = \int_T^0 dE \, \frac{1}{z_i^2 \, f\left(\frac{E}{m_i}\right)}, \tag{2.38}$$

so that:

$$\begin{aligned} R_2(T) &= \int_T^0 dE \, \frac{1}{z_2^2 \, f\left(\frac{E}{m_2}\right)} = \frac{z_1^2}{z_2^2} \int_T^0 dE \, \frac{1}{z_1^2 \, f\left(\frac{m_1}{m_2}\frac{E}{m_1}\right)} = \frac{z_1^2}{z_2^2}\frac{m_2}{m_1} \int_{\frac{m_1}{m_2}T}^0 dE' \, \frac{1}{z_1^2 \, f\left(\frac{E'}{m_1}\right)} \\ &= \frac{z_1^2}{z_2^2}\frac{m_2}{m_1} R_1\left(\frac{m_1}{m_2}T\right). \end{aligned} \tag{2.39}$$

Discussion

The simultaneous measurement of the stopping power dE/dx and of the particle momentum, or of its kinetic energy, or of its velocity, provides a tool to identify the particle type thanks to the scaling law of Eq. (2.37). The canonical example of a detector that allows for a simultaneous measurement of these quantities is the *time projection chamber* (TPC).

Suggested Readings

For an overview on the TPC, the reader is encouraged to consult the PDG review on detectors for accelerators [2]. See also Ref. [1] for the scaling law of stopping powers and ranges.

Problem 2.5 The range R of a particle is the distance over which the particle loses all of its kinetic energy. For a heavy ion, the energy loss per unit length of traversed material can be approximated by the formula

$$\frac{dE}{dx} = -\frac{C\,z^2}{\beta^2}, \tag{2.40}$$

where $C \approx 1.7$ MeV cm^{-1}, z is the ion charge in units of e, and β is the particle velocity.

- What kind of interaction between the ion and the material is responsible for this energy loss?
- Explain how the mass of a charged particle can be determined from the simultaneous measurement of dE/dx and of the momentum $|\mathbf{p}|$.

- Estimate the range R in water of a proton with $T = 60$ MeV.

Solution

As discussed in Sect. 2.1, heavy ions moving in matter lose energy due to elastic collision with the atomic electrons.

Since $dE/dx \sim z^2 f(\beta)$ and $|\mathbf{p}| = m\beta\gamma$, the simultaneous measurement of the two quantities allows to measure m for different ansatz on z. A comparison of the mass values thus obtained with the spectrum of known particles allows one to identify the particle type.

In order to estimate the range of a proton in water, we can use Eq. (2.35) obtained from the limit $\gamma \to 1$ in Eq. (2.32). We can obtain the same result starting from Eq. (2.40) and using the fact that $T = |\mathbf{p}|^2/2m$ for a classical particle:

$$R(T) = \int_T^0 dE\, \frac{1}{dE/dx} = \int_0^T dE\, \frac{\beta^2}{z^2\, C} = \int_0^T dT'\, \frac{2\,T'}{m_p\, c^2\, z^2\, C} = \frac{1}{m_p\, c^2}\, \frac{T^2}{z^2\, C} =$$
$$= \frac{(60)^2\ \text{MeV}^2}{10^3\ \text{MeV} \cdot 1^2 \cdot 1.7\ \text{MeV cm}^{-1}} = 2.1\ \text{cm}, \tag{2.41}$$

to be compared with a CSDA value of 3.1 cm from a full integration of the Bethe formula [5].

Bando n. 13153/2009

Problem 2.6 Discuss the characteristics of the Bragg peak and its main applications.

Solution

The energy loss of a charged ion in matter is described by the Bethe formula (2.1). Due to the dominant $1/\beta^2$ behaviour at velocities below about 0.9, the energy deposition per unit length becomes increasingly more intense as the particle velocity decreases. By tuning the initial particle energy T to attain a certain range R, the Bethe formula predicts that most of T will be infact dissipated near the end of the trajectory.

Since $E = E(\beta)$, the Bethe formula can be solved as an ordinary differential equation (ODE) in β, giving a solution $dE(x)/dx$. The latter features a peak at $x \approx R$, the so-called *Bragg peak*. Indeed, by using the approximation (2.3) and assuming the ion to be non-relativistic, the ODE can be easily solved analytically, yielding:

$$\frac{d}{dx}\left(\frac{1}{2}\, m\, \beta^2\right) = -\frac{z^2\, C}{\beta^2}, \qquad m\, \beta\, \frac{d\beta}{dx} = -\frac{z^2\, C}{\beta^2}, \qquad \beta^3\, d\beta = -\frac{z^2\, C}{m}\, dx,$$
$$\beta^4 - \beta_0^4 = -\frac{4\, z^2\, C}{m} x, \qquad \beta^2(x) = \beta_0^2 \sqrt{1 - \frac{4\, z^2\, C}{m\, \beta_0^4} x} = \beta_0^2 \sqrt{1 - \frac{x}{R}}, \tag{2.42}$$

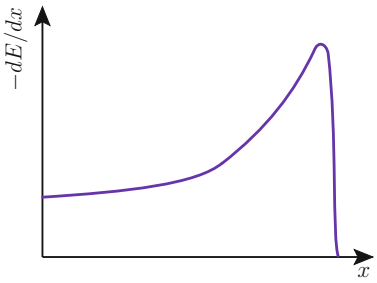

Fig. 2.4 Sketch of a typical Bragg curve for protons or heavy ions moving in a dense medium

where we have used Eq. (2.35) to define the range R of the particle. From Eq. (2.42) we therefore get:

$$\frac{dE}{dx}(x) = -\frac{z^2\,C}{\beta_0^2}\frac{1}{\sqrt{1-x/R}}. \tag{2.43}$$

The energy ΔE deposited in the interval $[\lambda R,\ R]$ can be easily computed from Eq. (2.43) to give:

$$\Delta E(\lambda) = \int_{\lambda R}^{R} dx \left|\frac{dE}{dx}\right| = T\sqrt{1-\lambda}. \tag{2.44}$$

The value of λ such that a fraction α of the initial energy is lost in the interval $[\lambda R,\ R]$ is therefore given by $\lambda = 1-\alpha^2$. For example, 50% of the kinetic energy T is lost in the last quarter of the particle path, and 25% in the trailing 6% of the path. A caveat: Eq. (2.43) has been obtained under the assumption that $dE/dx \sim \beta^{-2}$. This is a poor approximation for $\beta\gamma \lesssim 1$, and the resulting stopping power gets largely overestimated. Furthermore, when $\beta\gamma \lesssim 0.1$, the shell corrections are relevant, reducing significantly the stopping power, and the Bethe formula ultimately breaks down. Overall, the Bragg curve is much less peaked than predicted by Eq. (2.43), and infact the maximum occurs before the full range is attained, see Fig. 2.4.

The Bragg peak finds one major application in medical physics as a tool for curing solid tumors: the intense energy deposition in the neighbourhood of the beam range allows to burn selected tissue depths with reduced damage to the upstream tissue.

Bando n. 13705/2010

Problem 2.7 A 2 cm-thick plastic scintillator is coupled to a photomultiplier with gain $G = 10^6$ and detection threshold $Q_{\rm th} = 1$ pC, such that all the scintillation light can be assumed to be detected. A beam of particles of energy 10 GeV impinges perpendicularly to the scintillator:

- Estimate the charge collected at the anode, if the beam is made of muons.
- If the beam is made of neutrons, estimate the minimum scattering angle on protons such that the neutron can be detected.

Discussion

Scintillators have been briefly discussed in Sect. 2.1. A scintillator is always coupled with a photomultiplier that transforms the scintillating photons in photoelectrons (p.e.). Because of the geometry of the medium and of the QM-nature of the photoelectric effect, a photomultiplier is only sensitive to a fraction ε_C of the total light output, of which only a fraction ε_Q is actually converted into p.e. By themselves, such p.e. do not usually represent an amount of charge large enough to generate a significant signal, i.e. above the electronic noise. For this reason, the primary p.e. undergo a multiplicative enhancement between the photocathode and the anode. This can be for example achieved by accelerating them with intense electric fields, so that they can initiate a chain reaction that brings to the fan exponential charge multiplication. The enhancement factor, i.e. the total output charge per initial p.e., is the called *gain* (G) of the photomultiplier. The enhanced charge is finally read-out at the anode by a chain of amplifiers which transforms it into voltage or currents. A key point in all this procedure is that the proportionality between the initial number of p.e. and the final signal amplitude is preserved. After coupling the amplification stage to the read-out electronics, characterised by an electronic noise N_e, the relative energy resolution from a scintillator that produces n_γ Poisson-distributed photons for a particle of energy E, can be parametrised as [2]:

$$\frac{\sigma(E)}{E} = \sqrt{\frac{f_N}{n_\gamma\,\varepsilon_Q\,\varepsilon_C} + \left(\frac{N_e}{Q\,n_\gamma\,\varepsilon_Q\,\varepsilon_C}\right)^2}, \tag{2.45}$$

where f_N is the called *excess noise factor* and arised from the amplification process. The role of the gain factor in reducing the signal uncertainty is made clear by Eq. (2.45).

Solution

A 10 GeV muon loses energy mostly by collision with the atomic electrons as discussed in Sect. 2.1. In particular, it behaves as a MIP, and its mean energy loss per unit length is provided by Eq. (2.3). For a plastic scintillator, the mass density is approximately $\rho \approx 1$ g cm^{-3}. With this value, the energy loss is given by:

$$-\frac{dE}{dx} \approx 2.0\ \text{MeV g}^{-1}\ \text{cm}^2 \cdot 1\ \text{g cm}^{-3} = 2\ \text{MeV cm}^{-1}. \tag{2.46}$$

While crossing a thickness $d = 2$ cm, the total energy lost by the muon is $\Delta E = |dE/dx| \cdot d \approx 4$ MeV. The mean excitation energy for a plastic scintillator can be found in Table 2.2. Assuming $\varepsilon = 100$ eV, $\varepsilon_C = 1$, and $\varepsilon_Q = 1$, we expect to collect an average charge at the anode of about:

$$Q = G \cdot \frac{\Delta E}{\varepsilon} \cdot e = 10^6 \cdot \frac{4\ \text{MeV}}{100\ \text{eV}} \cdot 1.6 \times 10^{-19}\ \text{C} = 6.4\ \text{nC}, \tag{2.47}$$

i.e. more than three orders of magnitude larger than the threshold charge Q_{th}.

If the beam is made of neutrons, their detection proceeds through the measurement of the recoil energy of protons and other nuclei that interact with the beam particles. The threshold energy such that a recoil proton gives rise to a detectable signal is determined by the condition:

$$G \cdot \frac{T_{\text{th}}}{\varepsilon} \cdot e = Q_{\text{th}}, \quad \Rightarrow \quad T_{\text{th}} = \frac{10^{-12}\ \text{C} \cdot 10^2\ \text{eV}}{10^6 \cdot 1.6 \times 10^{-19}\ \text{C}} = 0.62\,\text{keV}, \tag{2.48}$$

which is small compared to the proton mass and to the beam momentum. It is easy to show that for very small recoil energy, momentum has to be exchanged perpendicularly. Indeed, if we indicated the four-momenta of the initial (final) neutron and proton by p and k (p' and k'), and the angle that the recoiling proton forms with the beam momentum as θ_p, then:

$$\begin{aligned} p' &= p + k - k', \\ m_n^2 &= m_n^2 + 2m_p^2 - 2E_n\, m_p - 2(E_n\, E'_p - |\mathbf{p}_n||\mathbf{p}'_p| \cos\theta_p) - 2E'_p\, m_p, \\ \cos\theta_p &= \frac{E'_p\,(E_n + m_p) - m_p\,(E_n + m_p)}{|\mathbf{p}_n||\mathbf{p}'_p|} = \frac{T_p\,(E_n + m_p)}{|\mathbf{p}_n||\mathbf{p}'_p|} \approx \\ &\approx \sqrt{\frac{T_p}{2m_p}} \left[\frac{E_n + m_p}{|\mathbf{p}_n|} \right], \quad \text{if} \quad |\mathbf{p}'_p| \ll m_p. \end{aligned} \tag{2.49}$$

Since $T \ll m_p$ for our case, and given that the factor within square brackets is of order one, the resulting angle turns out to be pretty much $\pi/2$, and conservation of momentum implies that the momentum received by the extra neutron is also is also a vector perpendicular to the beam direction. Since $T_{\text{th}} \ll E_n$, the neutron momentum magnitude after the scattering is almost unchanged, and the scattering angle of the neutron is therefore given by:

$$\theta_n \approx \frac{|\mathbf{p}'_p|}{|\mathbf{p}_n|} = \frac{\sqrt{2m_p T_{\text{th}}}}{|\mathbf{p}_n|} = \frac{\sqrt{2 \cdot 0.938 \cdot 0.62 \times 10^{-6}}}{10} = 1.1 \times 10^{-4}\,\text{rad}. \tag{2.50}$$

Bando n. 1N/R3/SUB/2005

Problem 2.8 A MIP generates, on average, n electron-ion pairs per cm in a gaseous detector at standard pressure. What is the typical value of n, if the gas consists in a argon-isobuthan mixture 60%–40%? Which additional factors acting on the statistics of the produced electrons determine the standard deviation of the signal?

Solution

On average, a MIP releases an amount of energy per unit length described by Eq. (2.3). If the gas is made of argon and isobutane, which have a small ionisation potential $I \approx 12\,\text{eV}$, see e.g. Table 6.1 of Ref. [1] or Ref. [5], the Bethe formula predicts an energy loss per mass surphace of about $2.5\,\text{MeV}\,\text{g}^{-1}\,\text{cm}^2$, see also Fig. 2.1. The density of the gas at STP conditions can be calculated from the law od ideal gases:

$$\rho = \frac{A}{R\,T/P} = \frac{(0.6 \cdot 18 + 0.4 \cdot 58)\,\text{g mol}^{-1}}{8.314\,\text{J mol}^{-1}\,\text{K}^{-1} \cdot 298\,\text{K}/10^5\,\text{Pa}} = \frac{34\,\text{g mol}^{-1}}{2.5 \times 10^4\,\text{cm}^3\,\text{mol}^{-1}} = \\ = 1.4 \times 10^{-3}\,\text{g cm}^{-3}. \tag{2.51}$$

The mean excitation energy for the two molecules can be read from Table. 2.2. Taking a weighted average of the two components, we get:

$$n = \frac{|dE/dx|}{(0.6 \cdot 26 + 0.4 \cdot 23)\,\text{eV}} = \frac{2.5\,\text{MeV}\,\text{g}^{-1}\,\text{cm}^2 \cdot 1.4 \times 10^{-3}\,\text{g cm}^{-3}}{24.8\,\text{eV}} = 140\,\text{cm}^{-1}. \tag{2.52}$$

In a gaseous ionisation detector, the primary electrons need to be accelerated by an intense electric fields until they trigger the formation of an avalanche. Indeed, an amount of primary ionisation electrons like in Eq. (2.52) is not sufficient to produce a detectable signal. Since the charge-multiplication process is intrinsically random, it introduces an additional fluctuation in the number of signal carriers. If an electron-ion pair recombines before the formation of the avalanche, or if it gets trapped by the gas molecules to give rise to an ion, it gets lost for later multiplication. Suitable amounts of electronegative gases, like freon, can limit this effect. The gain (see Problem 2.7), and hence the final statistics of signal carriers, depends on the choice of the gas. Noble gases are usually chosen because of their large gain factors. Another typical problem with gaseous detectors is the formation of avalanches in random points of the chamber created by energetic photons emitted by the accelerated electrons. This undesired effect limits the operation rate and resolution of the detector. These effects can be limited by adding appropriate amounts of organic quenchers, like isobutane. Finally, one should remember that the resolution of a gaseous ionisation detector that absorbs all of the particle kinetic energy scales better than $1/\sqrt{n}$ by the so-called *Fano factor*, which for typical gases is in the range $0.05 \div 0.20$, see e.g. Table 6.2 of Ref. [7].

Suggested Readings

An introduction to the physics of electronic avalanches in gas can be found in Refs. [1, 7]. For a more comprehensive review of gaseous detectors, the reader is addressed to Ref. [8].

Problem 2.9 How many electrons does a charged particle produce on average when crossing 100 μm of silicon?

Solution

Let us assume that the charged particle have $z = 1$ and that they behave like a MIP. The energy loss per unit length is given by the Bethe formula of Eq. (2.2). For a MIP, the dependence of dE/dx on the particle energy is mainly through the logarithmic term $\sim \ln \gamma$. Assuming the particle to be in the neighborhood of the global minimum, i.e. $\gamma \approx 4$, we can explicitly compute the right-hand side of Eq. (2.2) for a pure silicon medium, giving:

$$-\frac{dE}{dx} = \left(0.307\ \text{MeV mol}^{-1}\ \text{cm}^2\right) \cdot \frac{2.33\ \text{g cm}^3 \cdot 14}{28.1\ \text{g mol}^{-1}} \left[\ln \frac{2 \cdot 0.511\ \text{MeV} \cdot 4^2}{16 \cdot 14^{0.9}\ \text{eV}} - 1\right] = \\ = 3.7\ \text{MeV cm}^{-1}, \tag{2.53}$$

which agrees well with the more accurate prediction of $3.9\ \text{MeV cm}^{-1}$ [5]. The number of electron-hole pairs produced by the passage of such a particle across a thickness $d = 100$ μm of silicon is therefore given by:

$$n_{eh} = \frac{|dE/dx| \cdot d}{\varepsilon} = \frac{3.7\ \text{MeV cm}^{-1} \cdot 10^{-2}\ \text{cm}}{3.6\ \text{eV}} \approx 10^4, \tag{2.54}$$

where we have used the mean excitation energy for silicon as in Table 2.2.

Bando n. 1N/R3/SUB/2005

Problem 2.10 A relativistic electron loses energy by both ionisation and by radiation when moving inside matter.

- How does the energy loss by ionisation and by radiation depend on the material?
- How do they depend on the electron energy?
- The critical energy is defined as the energy at which the two energy losses are equal: which between a muon and an electron has the smallest critical energy?

Solution

The energy loss of relativistic electrons and positrons is discussed in Sect. 2.1. For energies below the critical energy E_c, energy loss by collision with the atomic electrons prevails. The material enters mostly through its electron density $n_e = N_A\, \rho\, Z/A$ and the average ionisation potential I. The stopping power is proportional to n_e and depends logarithmically on I. A residual dependence on the atomic number Z comes from the shell and density effects, see e.g. Ref. [2]. For electrons with energy in excess of a few MeV, the rate of energy loss by collision is almost independent of the electron energy, while it goes like T^{-1} at smaller energies.

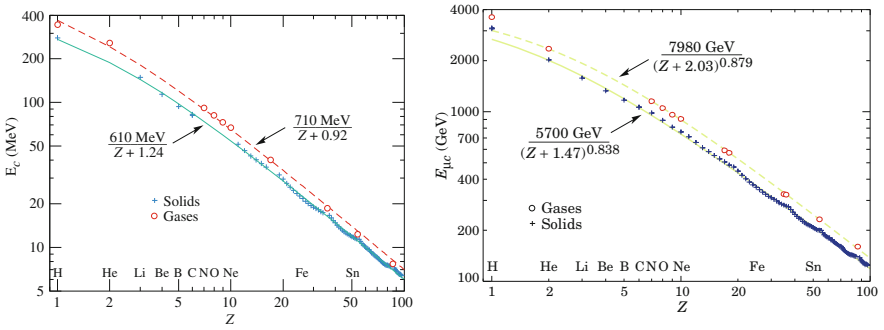

Fig. 2.5 Electron and muon critical energy for the chemical elements. From Ref. [2]

Energy loss by radiation prevails above the critical energy. The material enters through the atomic density $n = N_A\,\rho\,A$ and through the atomic number Z. In particular, it is proportional to the combination $Z^2\rho/A$, as shown by Eq. (2.13). Furthermore, it is proportional to the energy itself, see Eq. (2.12).

Since the energy loss by radiation is inversely proportional to m^2, where m is the mass of the incident particle, see Eq. (2.13), while the energy loss by ionisation is independent of m for sufficiently high energies, it follows that the critical energy must be approximately go as $\sim m^2$, since it is roughly given by the position of the intersection point between two curves in the $(dE/dx, E)$ plane, one of which is roughly constant (energy loss by collision), while the other (energy loss by radiation) is a straight line of slope proportional to m^{-2}. According to this picture, the critical energy for muons, $E_{\mu c}$, is expected to be about 4×10^4 times larger than for electrons. An exact scaling does not hold however, and the critical energy $E_{\mu c}$ is a factor of about 3 smaller than the naive scaling $E_{\mu c} \approx (m_\mu/m_e)^2\,E_c$, see e.g. Fig. 2.5 taken from Ref. [2].

Bando n. 13153/2009

Problem 2.11 An electron moving in a material loses energy by a variety of mechanisms. Define the critical energy and explain how it depends on the atomic number Z of the material.

Solution

Energy loss by collision and radiation are discussed in Sect. 2.1. The critical energy E_c is defined as the energy at which the two rates of energy loss become identical. An approximate formula for E_c is given by

$$E_c = \frac{800\,\text{MeV}}{(Z + 1.2)}, \tag{2.55}$$

see e.g. Ref. [1, 2]. Hence, the critical energy decreases with Z. In particular, it goes like Z^{-1} for $Z \gg 1$. This can be understood by the following argument: the critical energy is roughly given by the position of the intersection point between two curves in the $(dE/dx, E)$ plane, of which one is flat versus energy and goes like $\sim Z$ (energy loss by collision), while the other has a positive slope and goes approximately like $\sim Z^2$ at large values of Z (energy loss by radiation), hence the intersection point should scale as $\sim Z^{-1}$.

Bando n. 5N/R3/TEC/2005

Problem 2.12 Provide an approximate formula for the radiation length X_0 in terms of the atomic and mass numbers of the material.

Solution

An approximate version of X_0 has been derived in Eq. (2.13):

$$X_0 \approx \frac{716\ A}{Z\ (Z+1)\ \ln(287\ \sqrt{Z})}\ \mathrm{g\,cm^{-2}}, \tag{2.56}$$

where A is the mass number in units of $\mathrm{g\,mol^{-1}}$ and Z is the atomic number. Hence, the radiation length scales as $\sim A\ Z^{-2}$, for sufficiently large values of Z.

Bando n. 18211/2016

Problem 2.13 How much energy does an electron with initial energy of 1 GeV lose by crossing a material with thickness equal to one radiation length?

Solution

An energy of 1 GeV is above the critical energy E_c of Eq. (2.11), see Fig. 2.5, therefore the electron loses energy mostly by radiation. The rate of energy loss per unit length is therefore given by

$$\frac{dE}{dx} = -\frac{E}{X_0}, \tag{2.57}$$

where X_0 is the radiation length measured. The electron energy as a function of the traversed length is then obtained by integrating Eq. (2.57) to give:

$$E(x) = E_0\, e^{-x/X_0} \quad \Rightarrow \quad E(X_0) = \frac{E_0}{e} = 0.368\ E_0. \tag{2.58}$$

The energy lost in the medium is therefore $\Delta E = (1 - 1/e)\, E_0 = 0.632\, E_0$.

Bando n. 13153/2009

Problem 2.14 Determine the law by which a beam of electrons of intensity I_0 gets attenuated while crossing a layer of material of thickness d.

Solution

Electrons lose energy mostly by radiation at high energy, and then by elastic collison with atomic electrons at lower energies. If the beam is monochromatic and the thickness d exceeds the electron range in the material, the beam particles will traverse the full thickness and emerge with an energy distribution centred around a smaller value. Elastic scattering can instead deflect the electron from its original trajectory and remove it from the beam. Let's assume that the reaction which removes electrons from the beam is characterised by a cross section σ and let's denote the density of scattering centres by n. By definition, the probability of interaction per unit length is given by the interaction length of Eq. (1.291), namely $\lambda = 1/(n\sigma)$. If the beam has an intensity $I(x)$ at a depth x, the intensity at a distance $x + dx$ is given by:

$$I(x + dx) = I(x) - I(x)\frac{dx}{\lambda}, \qquad \frac{dI}{I} = -\frac{dx}{\lambda} \quad \Rightarrow \quad I(x) = I_0\, e^{-x/\lambda} \tag{2.59}$$

The intensity varies exponentially with the traversed length.

Bando n. 1N/R3/SUB/2005, Bando n. 13153/2009

Problem 2.15 In which energy interval does Compton scattering dominate in the interaction of photons with matter? What kind of interaction prevails at lower and higher energies? How does it depend on the absorber?

Solution

The interaction of photons with matter is discussed in Sect. 2.1. At low energy, the photoelectric effect (photon absorption with electron emission) is the main interaction mechanism. Compton scattering (incoherent photon-electron scattering) becomes significant for energies above the K-threshold and below a few times $2\, m_e$, after which pair-production dominates. The transition between the photoelectric and Compton-dominated regime depends on the medium (see below). For carbon (lead), the two become of similar size at energies of about 10 (500) KeV, see e.g. Ref. [2].

The absorber type enters mostly through the atomic number Z. The photoelectric cross section for energies in the MeV region is goes as $\sim Z^\beta$ with $\beta = 4 \div 5$. The Compton cross section is instead proportional to the number of electrons per atomi, hence it goes as $\sim Z$. The cross section for pair-production is inversely proportional to the radiation length X_0, hence it is roughly proportional to $\sim Z^2$ for large atomic numbers.

Suggested Readings

Photon interaction in matter is discussed in a large number of textbooks. For a primer, the reader is addressed to Sect. 2.7 of Ref. [1] and to the PDG review [2]. A large amount of tabulated data can be found in Ref. [6, 9].

Bando n. 5N/R3/TEC/2005

Problem 2.16 How does the photoelectric cross section vary as a function of the photon energy? How does it depend on the atomic number Z?

Solution

The interaction of photons with matter is discussed in Sect. 2.1. At low energy, the photoelectric effect (photon absorption with electron emission) prevails. The photoelectric cross section as a function of the photon energy features a number of edges corresponding to the opening of new atomic levels. For energies above the innermost level (K-shell), the cross section steeply falls with energy as $\sim E^{-7/2}$ and it grows with the atomic number as $\sim Z^{\beta}$ with $\beta = 4 \div 5$.

Suggested Readings

See Problem 2.15 and references therein.

Bando n. 18211/2016

Problem 2.17 Determine which process dominates in the photon-matter interaction for the following reactions:

1. 1 MeV photons on Al;
2. 100 keV photons on H_2;
3. 100 keV photons on Fe;
4. 10 MeV photons on C;
5. 10 MeV photons on Pb;

Solution

To solve this exercise, we can refer to Fig. 2.6, taken from Ref. [2], to read the cross section values for carbon and lead, and then use these values, together with the known Z-dependence of the cross sections, in order to extrapolate to other materials. To validate the extrapolation, we can use the values tabulated in Ref. [6].

1. A 1 MeV photon is just below the pair-production threshold. Aluminium has atomic number $Z = 13$. The energy at which Compton and pair-production become similar is about 500 keV in lead and about 10 keV in carbon. Aluminimum must be in-between, therefore Compton scattering has to be by far dominant at such an energy. Indeed, from Ref. [6] we find $\sigma_{\text{Comp}} \approx 3$ barn and $\sigma_{\text{p.e.}} \approx 10^{-3}$ barn.

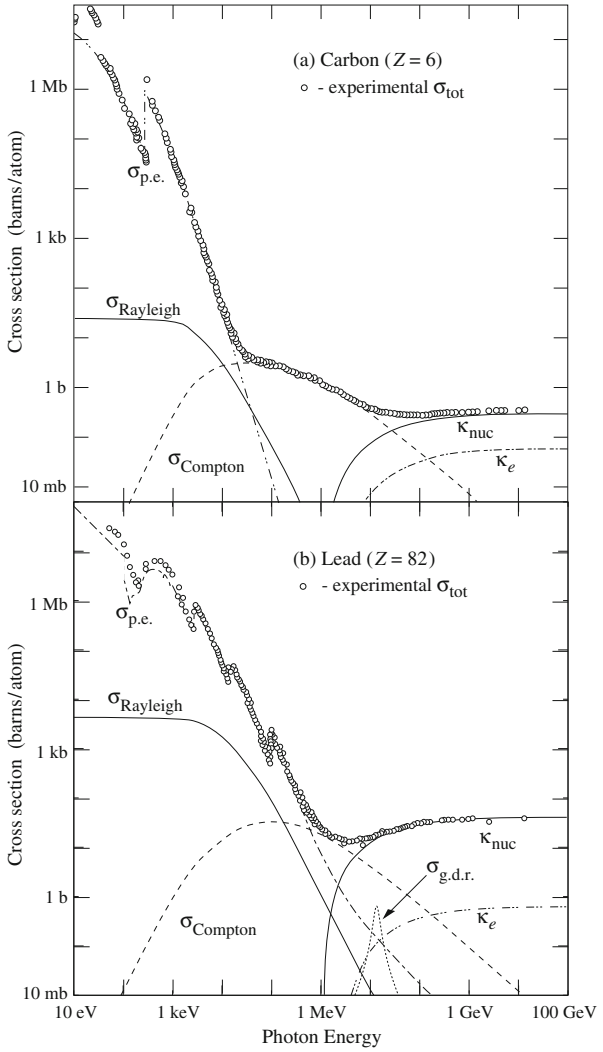

Fig. 2.6 Photon total cross sections as a function of energy in carbon and lead, showing the contributions of different processes. Taken from Ref. [2]

2. A 100 keV photon on hydrogen cannot undergo pair-production. Since Compton scattering dominates the photon-matter interaction at this energy for carbon, it will be *a fortiori* dominant in hydrogen, since the photoelectric cross section decreases as a function of Z much faster compared to the Compton cross section. Indeed, from Ref. [6] we find $\sigma_{\text{Comp}} \approx 0.5$ barn and $\sigma_{\text{p.e.}} \approx 10^{-6}$ barn.
3. A 100 keV photon on iron cannot undergo pair-production. From Fig. 33.15 of Ref. [2], the photoelectric (Compton) cross section in lead at that energy is around

10^3 barn (10 barn), so that, by assuming a $\sim Z^5$ ($\sim Z$) scaling, we should expect roughly the same cross sections. Indeed, from Ref. [6] we find $\sigma_{\text{Comp}} \approx 12$ barn and $\sigma_{\text{p.e.}} \approx 20$ barn.

4. A 10 MeV photon can undergo pair-production, but Compton scattering is sizable at that energy. Referring to Fig. 33.15 of Ref. [2], one sees that Compton cross section on carbon is larger than pair-production, although the two are still comparable. Indeed from Ref. [6] we find $\sigma_{\text{Comp}} \approx 0.3$ barn and $\sigma_{\text{pair}} \approx 0.8 \times 10^{-1}$ barn.
5. As before, one should expect the pair-production and Compton cross sections to be of the same order. This time, it's the former to be larger because of the $\sim Z^2$ scaling compared to just a $\sim Z$ scaling of Compton scattering. Indeed from Ref. [6] we find $\sigma_{\text{Comp}} \approx 4$ barn and $\sigma_{\text{pair}} \approx 12$ barn.

Bando n. 18211/2016

Problem 2.18 A muon with energy of 400 GeV penetrates vertically into the sea. By which process can it be detected? Estimate the depth at which the muon arrives before decaying.

Solution

A muon of energy $E = 400$ GeV moving in water ($n = 1.33$) emits Cherenkov radiation at a rate of about 200 γ/cm in the wavelength range [300, 500] nm, see Eq. (2.16).

The critical energy for electrons in water is about 80 MeV, see e.g. Ref. [5]. From the $\sim m^2$ scaling of the critical energy with the particle mass, the critical energy for muons is expected to be in excess of 3 TeV, hence far above the initial muon energy of 400 GeV. However, as discussed in Problem 2.10, the naive scaling is only approximate, and the critical energy for muons is about 1 TeV [5], hence still larger than the initial muon energy. From Fig. 33.24 of Ref. [2] we see that the critical energy for oxygen is about 900 GeV, so the same conclusions hold. The dominant energy loss mechanism is therefore by electron collision as described by the Bethe formula of Eq. (2.1). Since $\gamma = E/m = 3.8 \times 10^3 \gg 1$, we can use the approximate formula of Eq. (2.34) to predict the range R in water ($\rho = 1$ g cm^{-3}) to be $R \approx E/C$, where C is a constant that sets the plateau level of the Bethe formula. The stopping power for a MIP muon in water is about 2.0 MeV g^{-1} cm^2 [5]. However, at very large energies, the logarithmic term is non-negligible. Using the value $I = 80$ eV [5], the latter ranges from $\approx$26 at $\gamma = 3.8 \times 10^3$ down to $\approx$12 at $\gamma = 4$ (MIP). Taking an intermediate value of 20, the constant term can be approximated as $2.0 \times 20/12 \approx 3.3$ MeV g^{-1} cm^2. Therefore:

$$R \approx \frac{400\,\text{GeV}}{3.3\,\text{MeV g}^{-1}\,\text{cm}^2 \cdot 1\,\text{g cm}^{-3}} = 1.2\,\text{km}. \tag{2.60}$$

This result is in good agreement with the more accurate estimate of 1.216 km from Table II-28 of Ref [10]. However, the muon is an unstable particle with life-time

$\tau = 2.2 \times 10^{-6}$ s. The range calculation of Eq. (2.60) will hold only if the muon does not decay before coming to a stop. This is indeed the case with high probability. Although the muon momentum progressively changes as the muon penetrates deeper into the sea, time dilatation makes such that the muon decay probability over a fixed length in the Earth frame is significant only for small velocities. At a velocity $\beta = 0.94$, or $\gamma \approx 3$, the muon is at the minimum of the stopping power curve, and the residual energy is dissipated after traversing a length of about

$$\frac{106\,\text{MeV}}{2.0\,\text{MeV g}^{-1}\,\text{cm}^2 \cdot 1\,\text{g cm}^{-3}} \frac{(3-1)^2}{3} = 70\,\text{cm} \ll R. \tag{2.61}$$

Were the muon to conserve $\gamma = 3$, its mean path before decaying would be $\beta c \tau \gamma \approx 2$ km, so much larger than the residual path before stopping completely.

Discussion

The exploitation of large sea volumes as Cherenkov radiators allows one to study cosmic radiation of very high energy. For example, the IceCube neutrino observatory at the South Pole, is sensitive to the CC interaction of very-high energy neutrinos, which can be detected through their emission of Cherenkov light by an array of PMT's located deep into the ice.

Problem 2.19 An underground experiment located at a depth $d = 1$ km from the top of the mountain measures the momentum of cosmic muons arriving vertically from above. Estimate the muon energy at the top of the mountain if the muon momentum at the detector is $|\mathbf{p}| = 1.0$ TeV.

Solution

Energetic muons lose energy by electron collision and by various forms of electromagnetic radiation, including e^+e^- pair production, bremsstrahlung, and photonuclear interaction. The overall stopping power can be parametrised as

$$-\frac{dE}{dx} = a(E) + b(E)\,E, \tag{2.62}$$

where a and b are slowly varying functions of energy for $E \gtrsim 1$ TeV. Assuming constant values for a and b, Eq. (2.62) can be solved exactly to yield the solution $E_0 = E_0(E, x)$, namely:

$$\begin{cases} -\frac{dE}{dx} = a + b\,E \\ E(0) = E_0 \end{cases}$$

$$-\frac{dE}{a + b\,E} = dx, \qquad \ln\left(\frac{1 + E/E_{\mu c}}{1 + E_0/E_{\mu c}}\right) = -b\,x. \qquad E_0 = e^{b\,x}\left(E + E_{\mu c}\right) - E_{\mu c}, \tag{2.63}$$

where, by definition, $E_{\mu c} \equiv a/b$ is the energy at which energy loss by ionisation equals the energy loss by radiation. Using the values $a = 2.7\,\text{MeV g}^{-1}\,\text{cm}^2$ and $b = 3.9 \times 10^{-6}\,\text{g}^{-1}\,\text{cm}^2$ from Table 29.2 of Ref. [2], and by assuming the standard rock density $\rho = 2.65\,\text{g cm}^{-3}$, we get $E_{\mu c} = 0.69\,\text{TeV}$ and:

$$E_0 = \left(\exp\left[3.9 \times 10^{-6}\,\text{g}^{-1}\,\text{cm}^2 \cdot 2.65\,\text{g cm}^{-3} \cdot 10^5\,\text{cm}\right] \cdot 1.69 - 0.69\right)\,\text{TeV} = \\ = 4.0\,\text{TeV}. \tag{2.64}$$

Suggested Readings

For more details on cosmic muons and their interaction with matter, the reader is addressed to Sect. 29.4 and Sect. 33.6 of Ref. [2].

Problem 2.20 The vertical flux of cosmic muons with $E_\mu > 1\,\text{GeV}$ at the sea level is about $70\,\text{m}^{-2}\,\text{s}^{-1}\,\text{sr}^{-1}$, and the muon spectrum goes approximately as $E_\mu^{-2.7}$. Owing to the continuous slowing down and subsequent decay, the muon spectrum underground reduces with depth untill a depth of about 10 km w.e. (1 km w.e. $= 10^5\,\text{g cm}^{-2}$) is attained. At this point, the spectrum settles to a constant value. Explain this behaviour and provide a rought estimate of the muon flux deep underground.

Solution

At a depth d larger than a few km w.e., only muons with energies of order of $E_{\mu c}$ or larger can make their way through the underground soil, see Problem 2.19. In this energy regime, however, the range scales logarithmically with the muon energy at the sea level E_0:

$$R(E_0) \approx b^{-1} \ln\left(1 + \frac{E_0}{E_{\mu c}}\right), \tag{2.65}$$

where a and b are the constants introduced in Problem 2.19. Equation (2.65) implies an exponential suppression of the flux at large depths. At some point, the muon flux becomes so weak that another source of underground muons takes over, namely muon production from charged-current interaction of muon neutrinos with the rock. The latter is almost independent on the depth. For example, let's consider the infinitesimal flux of neutrinos with energy in the range $[E_\nu, E_\nu + dE_\nu]$: they will contribute to the measured muon flux of energy $E_\mu \geq E_{\text{th}}$, where E_{th} is the detector threshold energy, only if the muon interacts with the rock within a distance $r = R - E_{\text{th}}/(dE_\mu/dx)$ from the underground level d (we make the approximation $E_\mu \approx E_\nu$). The probability for such interaction is $r/\lambda \ll 1$, where λ is the interaction length and depends on the neutrino energy, see Eq. (1.291). For $E_{\text{min}} = 1\,\text{GeV}$, the offset $R - r$ is about 200 m. The neutrino spectrum can be assumed to be similar to the muon spectrum, since for every muon, a ν_μ of similar energy is produced, see Problem 1.19. The neutrino-induced flux can be thus estimated to be:

$$\Phi_\mu^{\text{deep}} \approx \int_{E_{\min}}^{E_{\max}} dE_\nu \, \frac{d\Phi_\nu^0}{dE_\nu} \left(\frac{R(E_\nu) - 200\,\text{m}}{\lambda(E_\nu)} \right) \tag{2.66}$$

The maximum energy $E_{\max}$ can be assumed to be of order of $E_{\mu c}$, since for larger energies the range becomes only mildly dependent on the muon energy, see Eq. (2.65), and thus it will contribute by one power less to the muon flux. Although the muon spectrum at $E_\mu \lesssim 10\,\text{GeV}$ decreases slower than $E_\mu^{-2.7}$, for an order-of-magnitude estimate we can assume for simplicity:

$$\frac{d\Phi_\nu^0}{dE_\nu} = (\alpha - 1)(1\,\text{GeV})^{\alpha-1} \Phi_0 \, E_\nu^{-\alpha}, \tag{2.67}$$

with $\Phi_0 = 70\,\text{m}^{-2}\,\text{s}^{-1}\,\text{sr}^{-1}$ and $\alpha = 2.7$. By using $dE_\mu/dx = 1.9\,\text{MeV}\,\text{g}^{-1}\,\text{cm}^2$ [5] and the cross section of Eq (1.354) for the neutrino-nucleon scattering (with $Q \approx 1$), and neglecting for simplicity the offset of 200 m, we have:

$$\begin{aligned} \Phi_\mu^{\text{deep}} &\sim \int_{1\,\text{GeV}}^{E_{\mu c}} dE_\nu \, \frac{d\Phi_\nu^0}{dE_\nu} \left(\frac{E_\nu}{1.9\,\text{MeV}\,\text{g}^{-1}\,\text{cm}^2 \cdot \rho} \right) \left(\frac{\rho \cdot N_A}{A} \cdot 1.6 \times 10^{-38}\,\text{cm}^2 \frac{E_\nu}{\text{GeV}} \right) = \\ &= \Phi_0 \cdot 0.23 \times 10^{-12} \left(\frac{\alpha - 1}{3 - \alpha} \right) \frac{(1\,\text{GeV})^{\alpha-1} \left(E_{\mu c}^{3-\alpha} - (1\,\text{GeV})^{3-\alpha} \right)}{\text{GeV}^2} \approx \\ &\approx 10^{-9}\,\text{m}^{-2}\,\text{s}^{-1}\,\text{sr}^{-1}. \end{aligned} \tag{2.68}$$

The result depends only mildly on the choice of $E_{\max}$. This order-of-magnitude estimate is in a decent agreement with the measured spectrum, see e.g. Fig. 2.7 taken from Ref. [2].

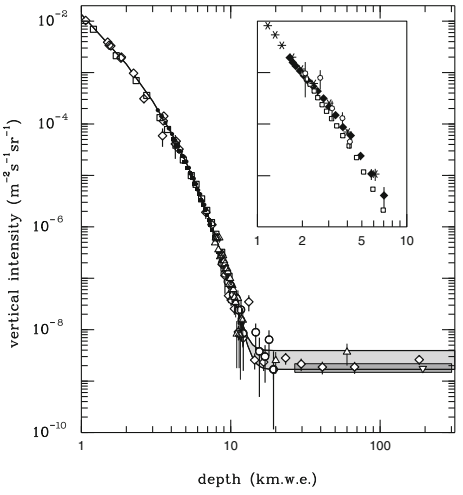

Fig. 2.7 Vertical muon intensity *versus* depth. From Ref. [2]

Suggested Readings

More details on cosmic ray fluxes, including a review of theoretical calculation, can be found in Ref. [11]. The reader is addressed to Sect. 29.4 of Ref. [2] for more details on the muon flux underground.

2.2 Particle Identification

Particle identification (PID) is a common problem in particle physics experiments, which are often equipped with a redundance of detectors as to be able to identify the particle type besides measuring their kinematics. As a general rule, the presence of backgrounds and imperfections in the detector makes PID a statistical test rather than a deterministic decision: the probability of correctly identifying a given particle (*efficiency*) has always to be weighted against the probability of wrongly identifying a background event (*fake-rate*). Depending on the particle type and on its energy, a variety of methods can be deployed in experiments. A non-exhaustive list of techniques for PID includes:

- *Measurement of the range*. Each particle loses energy by interaction with matter at a different rate, so that the measured range can be used to differentiate between different particle types. For example, a 10 GeV muon loses energy by collision at a MIP rate of about 11 MeV cm^{-1}, while an electron of the same energy loses energy by radiation at a rate of about 550 MeV cm^{-1}, i.e. about 50 times faster. Hadronic particles interact strongly with the nuclei, with typical interaction lengths of tens of centimetres for condensed materials. Therefore, the capability of muons to penetrate massive detectors exceeds by far larger that of other particles.
- *Measurement of the stopping power*. Even if the particle range is not fully contained within the active volume of a detector, the simultaneous measurement of the stopping power dE/dx and of the particle energy, or momentum, provides a handle to distinguish between different particles. The stopping power can be measured from the energy deposited within the detector. Time Projection Chambers, proportional chambers, nuclear emulsions, solid-state detectors are examples of detectors which can measure the energy loss across the particle trajectory.
- *Cherenkov-light detection*. Relativistic particles can emit Cherenkov lights when moving inside a refractive medium. The angle of emission and the number of emitted photons depend on the particle velocity β as for Eq. (2.15) and Eq. (2.21). A simultaneous measurement of the particle momentum and of the Cherenkov light can be thus used to determine the particle mass.
- *Transition-light detection*. For high-energy particles, Cherenkov detectors as particle identifiers become inefficient, see Eq. (2.21). An alternative to using the β-dependence of Cherenkov detectors is provided by the use of transition radiation detectors, which are sensitive to the light emitted by charged particles while

crossing the separation surface between vacuum and a dielectric material. Since the intensity of the emitted radiation is proportional to the γ-factor of the particle as for Eq. (2.22), particles of a given momentum, but very different mass, like pions and electrons, can be efficiently separated by measuring their transition light.

- *Measurement of the time-of-flight*. A simultaneous measurement of the particle momentum and of the TOF over known distances, allows to determine the particle mass. For unstable particles that decay in reconstructable vertices, the TOF can be measured from the distance traveled by the particle before decaying. Once combined with momentum information, this allows to infere the particle life-time (see Problem 1.32), and hence the particle type.
- *Kinematics*. In scattering experiments where the kinematics of the initial and final state can be measured, four-momentum conservation can be used to infere the mass of the particles involved in the scattering, see e.g. Problem 1.27, 1.28, and 1.62. For unstable particles, the kinematics of the decay products can be used to reconstruct the decay process, from which the mass of the mother particle can be inferred, see e.g. Problems 1.16, 1.20, 1.23, and 1.37.

Problems

Bando n. 13153/2009

Problem 2.21 Mention two methods of identification for charged particles, indicating the range of applicability and their complementarity.

Solution

At small velocities, the simultaneous measurement of the particle momentum $|\mathbf{p}|$ and of its time-of-flight over a known distance, or of the stopping power dE/dx, or of the Cherenkov light emission, represent canonical techniques for PID. However, at higher energies, all these methods become inefficient due to the saturation of the particle velocity to $\beta \to 1$, so that the TOF over a baseline distance L saturates to L/c for all particles, the stopping power (by collision) becomes only logarithmically sensitive to the particle velocity, while for Cherenkov detectors this is due to the fact that the sensitivity to mass differences is suppressed by $|\mathbf{p}|^{-2}$, see Problem 2.25.

At larger energies, one can instead exploit the emission of transition radiation, whose intensity is proportional to the γ-factor of the particle. High-energy electrons can be discriminated from other charged particles thanks to their larger emission of bremstrahlung radiation. In high-energy experiments, a combination of tracking and energy measurements in segmented calorimeters is sometimes used for PID: a calorimeter consisting of an electromagnetic (ECAL) and an hadronic (HCAL) section with independent read-out offers the possibility to separate electrons, which are stopped in ECAL, from hadrons, which interact in both. The attempt to reconstruct and identify each and every particle in a HEP event is called *particle flow* and was pioneered at LEP [12].

Suggested Readings

The PDG review of particle detectors at colliders provides a comprehensive and up-to-date overview of detectors for PID. Introductory textbooks like Ref. [13] are also indicated for a first overview on the subject. Besides the already quoted ALEPH publication [12], the reader is encouraged to read about PID within the particle flow algorithm as implemented in the CMS event reconstruction [14].

Bando n. 13153/2009

Problem 2.22 Discuss a few techniques for neutron detection as a function of the neutron energy.

Solution

Neutrons with energies in excess of a few GeV are best measured by hadronic calorimeters, i.e. devices that degrade the initial hadron energy by initiating a hadronic cascade and measure the visible energy deposited by the cascade particles, which is usually proportional to the incoming neutron energy, see Problem 2.35 for more details.

The detection of fast neutrons relies on the detection of the recoil proton in (n, p) scatterings. This is best achieved by using plastic or liquid organic scintillators, whose molecules contain hydrogen. Given the different fluorescent response of organic compounds to particles of different ionisation power, these materials can also offer n/γ discrimination by pulse-shape analysis.

For thermal neutrons, one usually relies on the nuclear reactions (n, γ) and (n, α), which can be e.g. detected by using liquid, glass, or inorganic scintillators, like Li I (Eu), or gaseous ionisation detectors, like ^{3}He, B F_3. The active material is conveniently loaded with suitable nuclei like ^{3}He, ^{6}Li, and ^{10}B, which have large cross sections for the reactions:

$$^3\mathrm{He}\,(n,\,p)\,\mathrm{t}, \qquad ^6\mathrm{Li}\,(n,t)\,^4\mathrm{He}, \qquad ^{10}\mathrm{B}\,(n,\alpha)\,^7\mathrm{Li}^{(*)}, \tag{2.69}$$

respectively. The kinetic energy of the emitted particles (protons, tritium, α-particles, Li ions) peakes at values determined by the Q-value of the reactions, thus allowing to separate the neutron signals from other backgrounds, most notably by photon interactions.

Suggested Readings

Chapter 7.7 of Ref. [1] describes the pulse-shape technique with scintillators and provides an introduction to various experimental techniques for neutron detection.

Bando n. 1N/R3/SUB/2005

Problem 2.23 In order to separate K^+ and π^+ in a momentum window between 700 MeV and 4 GeV, one can use two threshold Cherenkov detectors operated in series. Neglecting possible inefficiencies of the detectors near the threshold, determine which values of the refraction index can be chosen, and propose a suitable radiator.

Discussion

Although not mentioned explicitly, Cherenkov detectors are often integrated with spectrometers or other detectors that can measure the momentum of the particle. For example, Cherenkov detectors can be employed to select particles of a given type from a composite beam of given momentum.

Solution

The momentum acceptance of the experiment provides four threshold velocities and as many refraction indexes, namely:

$$\begin{cases} n < 1.0006 & \text{no } \pi \text{ emit} \\ n > 1.0195 & \text{all } \pi \text{ emit} \\ n < 1.0076 & \text{no } K \text{ emit} \\ n > 1.22 & \text{all } K \text{ emit} \end{cases} \tag{2.70}$$

With two counters at hand, one could set counter A at a value of $n_\mathrm{A} = 1.0195$, so that no signal there would imply that the particle is a kaon (K-tag), and counter B at a value $n_\mathrm{B} = 1.0076$, so that a signal in that counter would imply that the particle is not a kaon (π-tag). With this scheme one has three possibilities, summarised in Table 2.5. The third row (all counters with no-signal) represents a useful event only if the experiment is equipped with an independent trigger (e.g. a scintillator located along the beam direction). However, there remains an ambiguity for the case where only counter A records a signal. If one further assumes that the particle momentum can be measured, then the ambiguity is lifted. Indeed, if one considers pions and kaons with velocities in the range $[1/n_\mathrm{A}, 1/n_\mathrm{B}]$, the corresponding momenta span two non-intersecting ranges:

$$\frac{1}{n_\mathrm{A}} < \beta < \frac{1}{n_\mathrm{B}} \quad \Rightarrow \quad |\mathbf{p}| \in \begin{cases} [0.70,\ 1.12]\ \mathrm{GeV} & \pi \\ [2.49,\ 4.0]\ \mathrm{GeV} & K \end{cases} \tag{2.71}$$

so that a simultaneous measurement of the particle momentum and of the Cherenkov counters can discriminate between the two particles. Figure 2.8 shows the critical index $1/\beta$ for the two particle types as a function of $|\mathbf{p}|$. The dashed lines indicate the indexes chosen for counters A and B, while the vertical arrows mark the upper and lower momenta at which pions fail to generate a signal in B and kaons generate a signal in A, respectively. Concerning the choice of radiator medium, we can refer to Table 2.4 to identify possible candidates. In particular, we see that a value of $n - 1 \approx 2 \times 10^{-2}$ can be obtained for example by using aerogels, while $n - 1 \approx 7 \times 10^{-3}$ can

Table 2.5 Possible outcomes of a single-particle event using two threshold Cherenkov detectors in series with $N_A > n_B$

A	B	Particle
1	1	π
1	0	π or K
0	0	K
0	1	Not possible

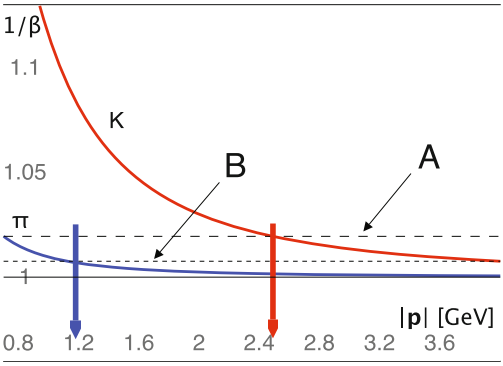

Fig. 2.8 The critical index $1/\beta$ for the two particle types as a function of $|\mathbf{p}|$. The dashed lines indicate the indexes chosen for counters A and B, while the vertical arrows mark the upper and lower momenta at which pions fail to generate a signal in B and kaons generate a signal in A, respectively

be obtained by using e.g. pentane (C_5H_{12}) or perfluoropentane (C_5F_{12}) of appropriate temperature and pressure.

Bando n. 13153/2009

Problem 2.24 Explain how the Cherenkov threshold depends on the refraction index of the medium. Three particles of different mass but same momentum $|\mathbf{p}|$ cross a system of two Cherenkov detectors arranged in series. How can the three particles be identified?

Solution

The Cherenkov threshold is the velocity β that equals the group velocity of light in the medium, i.e. $\beta = 1/n$, where n is the refraction index. By definition, vacuum has $n = 1$, and $n > 1$ for any other medium, see Table 2.4 for a few representative materials.

Given two threshold Cherenkov detectors A and B operated in series, the identification of three particles of different mass but same momentum $|\mathbf{p}|$, such that the three particles have velocities $\beta_1 < \beta_2 < \beta_3$, can be achieved by setting the refraction index of the two counters at $n_A = 1/\beta_1$ and $n_B = 1/\beta_2$, so that:

- particle (1) is below threshold in both counters ($\beta_1 \leq 1/n_A,\ 1/n_B$), thus producing no signal in any of the two counters.

- particle (2) is above threshold in counter A ($\beta_2 > 1/n_\mathrm{A}$), but below threshold in counter B ($\beta_2 \leq 1/n_\mathrm{B}$), thus producing a signal in only one counter;
- particle (3) is above threshold ($\beta_3 > 1/n_\mathrm{A},\ 1/n_\mathrm{B}$) in both detectors, thus producing a signal in both counters;

An analysis of the signal output in the two counters can thus reveal which of the three particles has crossed the detector. This configuration also maximises the light yield when the particle is above threshold.

Problem 2.25 A Cherenkov imaging detector measures the angle θ of Cherenkov photons with a resolution $\sigma_\theta = 2\,\mathrm{mrad}$. What is the largest beam momentum $|\mathbf{p}|$ such that kaons and pions can be discriminated to better than 3σ by the angular measurement only, if the Cherenkov radiator consists of fused silica ($n = 1.474$) or fluorocarbon gas ($n = 1.0017$)?

Solution

Let the Cherenkov angle be denoted by θ. A separation to better than 3σ amounts to require $\Delta\theta/\sigma_\theta \geq 3$. By approximating finite differences by their differentials, we get:

$$\frac{\Delta\theta}{\sigma_\theta} \approx \frac{d\theta}{\sigma_\theta} = \frac{1}{\sigma_\theta \sin\theta} d\cos\theta = \frac{\beta}{\sigma_\theta\sqrt{\beta^2 n^2 - 1}} d\left(\frac{1}{\beta}\right) = \frac{\beta^2\, dm^2}{2\,\sigma_\theta\sqrt{\beta^2 n^2 - 1}\,|\mathbf{p}|^2}$$
$$\approx \frac{|m_K^2 - m_\pi^2|}{2\sigma_\theta\sqrt{n^2-1}|\mathbf{p}|^2}. \tag{2.72}$$

Hence, the largest momentum for which the statistical separation is in excess of $N_\sigma = 3\sigma$ is provided by:

$$|\mathbf{p}| < \frac{|m_K^2 - m_\pi^2|}{\left[N_\sigma \cdot 2\sigma_\theta\sqrt{n^2-1}\right]^{\frac{1}{2}}} = \begin{cases} \frac{0.474\ \mathrm{GeV}}{\sqrt{3\cdot 2\cdot 2\times 10^{-3}\cdot\sqrt{1.474^2-1}}} = 4.2\,\mathrm{GeV} & \text{silica} \\ \frac{0.474\ \mathrm{GeV}}{\sqrt{3\cdot 2\cdot 2\times 10^{-3}\cdot\sqrt{1.0017^2-1}}} = 18\,\mathrm{GeV} & \text{fluorocarbon} \end{cases} \tag{2.73}$$

Suggested Readings

This problem is inspired by Sect. 34.5 of Ref. [2]. The reader is addressed to this reference for more information on the subject.

Problem 2.26 Tellurium dioxide ($\mathrm{Te\,O_2}$) crystals ($n = 2.4$, $\rho = 6\,\mathrm{g\,cm^{-3}}$) have been used to search for the putative neutrinoless double-beta decay ${}^{130}_{52}\mathrm{Te} \rightarrow {}^{130}_{54}\mathrm{Xe}$ in bolometric calorimeters. The experimental signature is provided by an energy deposit around 2.53 MeV. A major background to this process is represented by α-decays of radioactive contaminants. Show that the simultaneous measurement of Cherenkov photons and calorimetric energy would allow to separate α particles from signal events. Estimate the mean number of Cherenkov photons with wavelengths in the range [350, 600] nm produced by a signal event in a few centimetres long crystals.

Discussion

Differently from an ordinary double-β decay ($2\nu\beta\beta$), where a nucleus ${}^{A}_{Z}X$ decays to ${}^{A}_{Z+2}Y + 2\nu + 2e^-$, a neutrinoless double-$\beta$ decay ($0\nu\beta\beta$) does not produce neutrinos in the final state. The Q-value of the reaction, see Problem 1.39, is entirely taken by the two electrons: their energy sum is therefore a line around Q smeared by the detector resolution. This also implies that the electron energies are fully anticorrelated. The theoretical energy distributions for this decay can be found in Ref. [15]. Alpha particles of a few MeV energy, typical of radioactive decays, behave like background events by releasing their energy in the calorimeter.

Solution

In order to prove that the electrons radiate Cherenkov light while the α particles do not, it suffices to verify that the threshold velocity $\beta = 1/n = 0.717$ in $\mathrm{Te\,O_2}$ is above the velocity of α's, but below the velocity of at least one of the electrons. Assuming $T_\alpha = 2.53\,\mathrm{MeV}$, one has

$$\beta_\alpha \approx \sqrt{\frac{2T_\alpha}{m_\alpha}} = \sqrt{\frac{2 \cdot 2.53\,\mathrm{MeV}}{3.73\,\mathrm{GeV}}} = 0.037 < \beta, \tag{2.74}$$

while for a $0\nu\beta\beta$ decay:

$$\max \beta_e > \sqrt{1 - \left(\frac{m_e}{Q/2 + m_e}\right)^2} = \sqrt{1 - \left(\frac{0.511\,\mathrm{MeV}}{1.77\,\mathrm{MeV}}\right)^2} = 0.958 > \beta. \tag{2.75}$$

To good approximation, the total range and the number of Cherenkov photons are independent of the energy sharing between the two electrons, thanks to the anticorrelation between the two energies. Indeed, for $\gamma \gg 1$, the range is a linear function of energy as for Eq. (2.32). In the case of interest, though, the average kinetic energy is comparable to m_e, so the linearity is lost. However, a numerical investigation shows that the total range is constant to within 15% over the allowed electron spectrum, and is larger when the energy sharing is more asymmetric. Furthermore, Eq. (2.32) is expected to underestimates the true range for small values of γ, and one should rather use the full calculation. To circumvent the lack of tabulated data and the mild dependence on the kinematics, we consider a particular decay configuration,

namely $T_1 = 1.0\,\text{MeV}$ and $T_2 = Q - T_1 \approx 1.5\,\text{MeV}$. We then approximate the stopping power by averaging the tabulated values for two similar materials: Na I, which contains Iodine, a Tellurium neighbour in the periodic table, and $\text{Ti}\,\text{O}_2$, which is also a metal dioxide. At $T = 1\,\text{MeV}$, Ref. [16] gives:

$$R_1(\text{Na I}) = 0.69\,\text{g}\,\text{cm}^{-2}, \qquad R_1(\text{Ti}\,\text{O}_2) = 0.55\,\text{g}\,\text{cm}^{-2}, \tag{2.76}$$

Taking the mean, we get $R_1 \approx 0.64\,\text{g}\,\text{cm}^{-2}$, or 0.10 cm. There are no values tabulated for $T = 1.5\,\text{MeV}$, but we can use the scaling predicted by Eq. (2.32), giving a ratio $R_2/R_1 = 1.69$. Hence, $R_2 \approx 0.175\,\text{cm}$. The light output in the wavelength window [350, 600] nm can be estimated by using Eq. (2.16) with $\langle \sin^2\theta \rangle \approx 1 - 1/n^2$, giving:

$$\begin{aligned} N_\gamma &\approx (0.10 + 0.175)\,\text{cm}\,\frac{1.15 \times 10^3\,\text{cm}^{-1}}{\sqrt{600 \cdot 350}/400}\left(1 - \frac{1}{2.4^2}\right)\frac{600 - 350}{\sqrt{600 \cdot 350}} \\ &= 46 + 79 = 125, \end{aligned} \tag{2.77}$$

which agrees with the more accurate expectation of Ref. [17], which averages the range over the proper energy spectrum.

Suggested Readings

The idea of exploiting Cherenkov radiation in bolometric detectors has been first proposed in Ref. [17], from which the problem is largely inspired.

Problem 2.27 A threshold Cherenkov detector is used to separate muons from pions in a beam with momentum $|\mathbf{p}| = 150\,\text{MeV}$. What values of the refraction index n can be used?

Solution

The condition for which muons emit Cherenkov light, while pions do not, is given by:

$$1/\beta_\mu < n < 1/\beta_\pi \quad \Leftrightarrow \quad \sqrt{\left(\frac{m_\mu}{|\mathbf{p}|}\right)^2 + 1} < n < \sqrt{\left(\frac{m_\pi}{|\mathbf{p}|}\right)^2 + 1},$$

giving the result: $1.22 < n < 1.37$.

Bando n. 1N/R3/SUB/2005

Problem 2.28 An experiment needs to distinguish pions from kaons of momentum $|\mathbf{p}| = 2\,\text{GeV}$ by measuring the time flight on a $L = 2\,\text{m}$ baseline. The instrumentation has a time resolution $\sigma_t = 0.2\,\text{ns}$. Can each particle be identified? With which precision can the pion fraction be determined?

Solution

The time-of-flight (TOF) for pions and kaons in the beam is given by:

$$t = \frac{L}{\beta c} = \frac{L}{c}\sqrt{1+\frac{m^2}{|\mathbf{p}|^2}} = \frac{2\,\mathrm{m}}{3\times 10^8\,\mathrm{m\,s^{-2}}} \begin{cases} \sqrt{1-\left(\frac{0.139}{2}\right)^2} = 6.68\,\mathrm{ns} & \pi \\ \sqrt{1-\left(\frac{0.494}{2}\right)^2} = 6.87\,\mathrm{ns} & K \end{cases} \tag{2.78}$$

Since $\Delta t = 0.19\,\mathrm{ns} \approx \sigma_t$, particle-by-particle identification is affected by a large statistical uncertainty, i.e. the Type-II error is large for any given efficiency to identify the correct particle type. For example, if we decided to tag a particle as a K if the TOF is in excess of $6.87 - 1\sigma_t = 6.67\,\mathrm{ns}$, the selection efficiency would be 84%, for a fake-rate of about 50%. Even though an event-by-event classification is not very accurate, the pion (or kaon) fraction of the beam can be estimated with large accuracy for a sufficiently large number of measurements. Assuming N independent and gaussian distributed measurements $\mathbf{X} = \{X_i\}$, the maximum-likelihood (ML) estimator of the pion fraction $\bar{\varepsilon}_\pi$ is given by the solution of the equation:

$$0 = \left.\frac{\partial L(\mathbf{X},\varepsilon_\pi)}{\partial \varepsilon_\pi}\right|_{\hat{\varepsilon}_\pi},$$
$$\text{with} \quad L = \prod_{i=1}^{N} f(X_i,\varepsilon_\pi) = \prod_{i=1}^{N} \left[\varepsilon_\pi\, \mathcal{N}(X_i \mid t_\pi,\sigma_t) + (1-\varepsilon_\pi)\, \mathcal{N}(X_i \mid t_K,\sigma_t)\right] \tag{2.79}$$

The classical theory of estimators predicts that the asymptotic variance of the ML estimator is given by

$$\mathrm{Var}\left[\hat{\varepsilon}_\pi\right] = \frac{1}{N\, I(\hat{\varepsilon}_\pi)}, \qquad \text{with} \quad I(\hat{\varepsilon}_\pi) = \mathrm{E}\left[-\frac{\partial^2 \ln f(x,\varepsilon_\pi)}{\partial^2 \varepsilon_\pi}\right], \tag{2.80}$$

see Sect. 4.1. The information can be computed numerically using a simple program for different values of ε_π, see Appendix 2.3. The result is a number of $\mathcal{O}(1)$: for example, for $\varepsilon_\pi = 0.1$ (0.3) one gets $I = 1.03$ (0.80). Hence, the standard deviation on the pion fraction will be given by:

$$\sigma_{\hat{\varepsilon}_\pi} \approx \frac{1}{\sqrt{N}}. \tag{2.81}$$

Problem 2.29 In 1987, the water Cherenkov detector Kamiokande-II in the Kamioka mine (Japan), detected a neutrino burst that was attributed to a supernova event occurred at a distance $d = 5.5\times 10^4$ kpc from the Earth. The energy and arrival time at the detector could be measured for those (anti)neutrinos that interacted via the charged-current (CC) scattering $\bar{\nu}\, p \to n\, e^+$, or by the electron-scattering (ES)

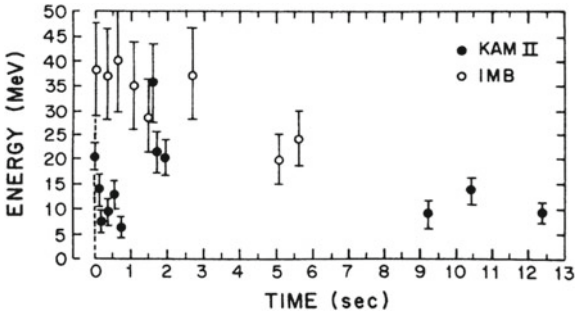

Fig. 2.9 Scatter plot of energy and time for the twelve supernova candidate events recorded by Kamionkande in 1987 (from Ref. [18])

reaction $\nu_e\, e^- \to \nu_e\, e^-$, within the fiducial volume of the detector. During a time interval $\Delta t = 12$ s, a total of 12 events were registered. The time *vs* energy diagram of the signal events is reported in the Fig. 2.9.

- The Kamiokande experiment could not distinguish electrons from positrons by using the sole Cherenkov light. How was it then possible to separate ν_e from $\bar{\nu}_e$?
- Explain how the antineutrino energy $E_{\bar{\nu}}$ could be measured from the positron energy E_{e^+}.
- Determine a lower bound to the ν_e lifetime.
- Using the data reported in the plot, estimate an upper bound to the electron neutrino mass m_{ν_e}.

Discussion

As of 1987, the Kamiokande-II experiment consisted of a cylindric water tank containing over 2000 t of water instrumented with uniformly distributed PMT's covering about 20% of the total surface. The PMT's were sensitive to the Cherenkov light in the range $300 \div 500$ nm. At these wavelengths, the light attenuation length exceeds 50 m, thus allowing an efficient light collection all across the fiducial volume. The event trigger, production vertex, direction, and energy of the particles were reconstructed by using the charge and time stamp of all PMT with a signal above the noise. The single-PMT time resolution was 13 ns, while the relative energy resolution was estimated from simulation to be about 20%. An electron neutrino with energy of about 10 MeV interacts mostly through ES on the atomic electrons. The CC interaction with the transmutation ${}^{16}_{6}\mathrm{O} \to {}^{16}_{7}\mathrm{F}$ is instead suppressed by the large mass difference $\mathscr{B}({}^{16}_{6}\mathrm{O}) - \mathscr{B}({}^{16}_{7}\mathrm{F}) \approx 16$ MeV. Conversely, an electron antinutrino interacts mostly through the CC reaction $\bar{\nu}\, p \to n\, e^+$, provided $E_{\bar{\nu}} \gtrsim 2$ MeV. The main background to $\sim$10 MeV electrons and positrons is represented by cosmic muons, β-decays of unstable isotopes polluting the water, and by γ/n radiation from the cavern walls.

Solution

The separation between electrons and positrons is possible on a statistical basis. Indeed, the CC scattering for antineutrino energies $E_{\bar{\nu}} \approx 10$ MeV is isotropic in the laboratory frame. This can be proved as follows. First, one notices that the velocity of

the centre-of-mass frame is $\beta = E_{\bar{\nu}}/(E_{\bar{\nu}} + m_p) \approx 10^{-2}$, so that the centre-of-mass is almost at rest in the laboratory frame. In the latter, the dynamics is governed by the exchange of a virtual W boson, as described by the Fermi Lagrangian:

$$\mathscr{L}_{\mathrm{F}} = \frac{G_{\mathrm{F}}}{\sqrt{2}} \cos\theta_{\mathrm{C}} \left[\bar{n}\gamma_\mu(1-\alpha\gamma_5)p\right]\left[\bar{\nu}\gamma^\mu(1-\gamma_5)e\right]. \tag{2.82}$$

The amplitude squared can be obtained with the usual Casimir's tricks. By taking $\alpha = -1$, it becomes proportional to $(p_{e^+}p_p)(p_{\bar{\nu}}p_n) \approx E_{e^+}E_{\bar{\nu}}m_p m_n$, if the neutron recoil is neglected compared to the nucleon mass. In this case, E_{e^+} is also a constant, hence the ampitude squared itself is constant. From Problem 1.53 and the considerations above, we can see that the cross section is roughly isotropic in the laboratory frame. This is not the case for the ES, since the centre-of-mass velocity is now $\beta = E_{\bar{\nu}}/(E_{\bar{\nu}} + m_e) \approx 1$. which gives rise to a very forward-peaked differential cross section in the laboratory frame, see Problem 1.15.

For the antineutrino scattering, energy conservation implies

$$E_{\bar{\nu}} + m_p = E_{e^+} + m_n \quad \Rightarrow \quad E_{\bar{\nu}} \approx E_{e^+} + \underbrace{(m_n - m_p)}_{1.3\ \mathrm{MeV}}. \tag{2.83}$$

The neutrino lifetime, τ_ν, has to be large enough so that the neutrinos can make it to Earth, i.e.:

$$\tau_\nu \gtrsim \frac{d}{c\,\gamma_\nu} = \frac{5.5\times10^4\ \mathrm{pc}}{c\,(E_\nu/m_\nu)} = \frac{5.5\times10^4\cdot 3.3\ c\cdot\mathrm{y}}{c\,(E_\nu/m_\nu)} = 1.8\times10^5\left(\frac{m_\nu}{E_\nu}\right)\mathrm{y}, \tag{2.84}$$

where we have used the relation $1\ \mathrm{pc} \approx 3.3\ c\cdot\mathrm{y}$.

If the neutrino burst starts at the time $t = 0$, the arrival time at the detector is:

$$t = \frac{d}{\beta_\nu c} = \frac{d}{c}\frac{1}{\sqrt{1-(m_\nu/E_\nu)^2}} \approx \frac{d}{c}\left[1+\frac{1}{2}\left(\frac{m_\nu}{E_\nu}\right)^2\right]. \tag{2.85}$$

Two neutrinos of energies E_1 and E_2, emitted at the same time $t = 0$, will arrive at destination with a time separation:

$$t_1 - t_2 = \frac{d}{2c}m_\nu^2\left(\frac{1}{E_1^2} - \frac{1}{E_2^2}\right). \tag{2.86}$$

From the recorded data, we observe the presence of a few neutrino events separated by about 10 s from the the first burst events, which is larger than the expected duration of a supernova burst (a few seconds), is an indication that neutrinos have a mass, since otherwise they would have arrived all in one shot. The presence of two populations of events, one located within the first second, and the other around $t = 2$ s, which are not distributed according to Eq. (2.85), indicates, though, that the pattern of

neutrino emission from the supernova has some non-trivial time dependence, i.e. one cannot assume a perfectly synchronous burst. Yet, some of the neutrinos must have been created simultaneously, and with some broad spectrum of energies, so that any difference in arrival time has to be attributed to the non-zero neutrino mass. A conservative upper limit on m_ν can thus be obtained by considering, those events that feature the largest energy difference $|\Delta E|$ among the first and last arrived events, respectively. From the plot, we take e.g.: $(E_1, t_1) = (35\,\text{MeV}, 1.5\,\text{s})$ and $(E_2, t_2) = (10\,\text{MeV}, 12.5\,\text{s})$. Inverting Eq. (2.86), we have:

$$m_\nu \lesssim \sqrt{\frac{2c\,(t_1 - t_2)}{d}}\,\frac{E_1\,E_2}{\sqrt{E_2^2 - E_1^2}} \approx 20\,\text{eV}. \tag{2.87}$$

Suggested Readings

This problem is inspired by the Kamiokande publication of Ref. [18].

Bando n. 18211/2016

Problem 2.30 A ν_μ beam with an energy of 30 GeV enters a detector containing liquid Ar. A fraction of the events features a few metres long track starting from the interaction point, while, for a smaller fraction of the events, all tracks are contained within a small volume. Explain this behaviour.

Solution

As already discussed in Problem 1.64, neutrinos can undergo interactions with both the nuclei and and the atomic electrons, the latter having a cross section suppressed by a factor of m_e/m_N. In both cases, the neutrinos can interact via either the charged current, $\nu_\mu\,X \to \mu^-\,Y$, or the neutral current interaction, $\nu_\mu\,X \to \nu_\mu\,X'$. The EWK theory predicts the ratio between neutral and charged current cross section in terms of the Weinberg angle θ_W to be:

$$\left(\frac{\sigma_\text{NC}}{\sigma_\text{CC}}\right)_\nu = \frac{1}{2} - \sin^2\theta_\text{W} + \frac{20}{27}\sin^4\theta_\text{W} \approx 0.31, \tag{2.88}$$

see e.g. Ref. [19]. When a neutrino of energy $E_\nu = 30\,\text{GeV}$ interacts via CC, it produces a muon of similar energy, which being a MIP, is highly penetrating in the Ar medium and can be therefore identified as a long track. Conversely, in the occurrence of a NC interaction, the only detectable signal is provided by the recoil of the struck nucleus. Since DIS prevails in this energy regime, the interaction is inelastic and results in a number of hadronic particles which, being much heavier than the muon and less energetic, have smaller range, thus appearing as a set of short tracks emerging from the interaction point.

Suggested Readings

The reader is addressed to Chap. 12 of Ref. [19] for more information on neutrino interactions in matter.

Problem 2.31 A charged particle is moving inside a uniform magnetic field of intensity $B = 1.0\,\mathrm{T}$. The radius of curvature of the track is $R = 7.25\,\mathrm{m}$ with negligible error. The kinetic energy of the particle is measured to be $T = (2.00 \pm 0.03)\,\mathrm{GeV}$. Determine which type of particle is most probably being measured.

Solution

The charge sign is fixed by the direction of curvature. The particle momentum $|\mathbf{p}|$ is instead given by the formula:

$$|\mathbf{p}| = 0.3\,|z|\ (B/\mathrm{T})\ (R/\mathrm{m})\ \mathrm{GeV} = 2.20\,|z|\,\mathrm{GeV}, \tag{2.89}$$

where z is the particle charge in units of the proton charge e, see Problem 3.3. The particle mass m is therefore given by:

$$m^2 = (T+m)^2 - |\mathbf{p}|^2, \qquad m = \frac{|\mathbf{p}|^2 - T^2}{2T} = \frac{(2.20\cdot z)^2 - (2.00)^2}{2\cdot 2.00}\,\mathrm{GeV}. \tag{2.90}$$

The uncertainty on m can be obtained by propagating the uncertainty on T:

$$\Delta m = \left|\frac{\partial m}{\partial T}\right| \Delta T = \frac{1 + |\mathbf{p}|^2/T^2}{2}\,\Delta T = \frac{1 + (2.20\cdot z/2.00)^2}{2}\cdot 0.03\,\mathrm{GeV}. \tag{2.91}$$

Stable, non-exotic particles have integer charges. We can therefore try different *ansatz* values of $|z|$ and compare the result with the known spectrum of particles. For $|z| = 1$, Eq. (2.90) gives $m = (210 \pm 30)\,\mathrm{MeV}$, which does not match any known particle within the experimental uncertainty. For $|z| = 2$, one has $m = (3.84 \pm 0.09)\,\mathrm{GeV}$, which is compatible with the mass of the α particle $m_\alpha = 3.73\,\mathrm{GeV}$ at the 1σ level.

Bando n. 13153/2009

Problem 2.32 Describe which methods could be used to measure lifetimes of order 10^9 years, 10^{-12} s, and 10^{-22} s.

Solution

Lifetimes of order 10^9 years are typical of radioactive decays. Such lifetimes can be measured by counting the number of decays in a sample and in a given time interval Δt. Let N_C be the number of countings after background-subtraction. Under the assumption $\tau \gg \Delta t$, the lifetime can be measured from the relation:

$$\tau = \frac{V\,\rho\,N_{\mathrm{A}}}{A}\frac{\Delta t}{N_C}, \tag{2.92}$$

where V is the volume of the sample being observed.

Lifetimes of order 10^{-12} s are characteristics of weakly decaying particles, like D and B mesons, or τ leptons. Since $c = 3 \times 10^2$ μm/ps, the decay vertexes of such particles are of order 300 μm, when the particles are produced at relativistic energies. Silicon detectors, with intrinsic spatial resolutions of a few tens of microns or better, see Problem 2.43, are ideal candidates to build vertex detectors with sufficient resolution to resolve such decays.

Lifetimes of 10^{-22} s are characteristics of strongly decaying particles, like the ρ and ω mesons, or the Δ baryon. The distance of flight is far too small to be measurable by any position-measuring device. Such lifetimes are therefore indirectly estimated from the decay width Γ of Eqs. (1.186), as measured from the invariant mass distributions of the decay products, or from the production cross section.

2.3 Functioning of Particle Detectors

Particle detectors record the passage of particles. Depending on the detector type and on the form of radiation it is sensitive to, detectors can be used to measure the position and time of arrival of a given particle at the detector location, the energy and direction of the incoming particle, and sometimes even identify the type of particle. Detectors are usually composed of an active volume, which interacts with the particle, and a readout component, hosting the electronics required to generate an electric signal, provide signal amplification to improve the signal-over-noise ratio, and finally shape the signal according to some logic suitable for later processing in the experiment or for persistent data storage. In modern experiments, detectors are commonly operated by computers, which supervise their correct functioning and take care of data acquisition. The field of particle detection is vast and finds application that range from pure research to industry. No attemp is made here to give a comprehensive overview on this subject. The selected problems want to discuss the main technologies and introduce general concepts, like resolution, efficiency, dead time.

Problems

Bando n. 1N/R3/SUB/2005

Problem 2.33 In an electromagnetic calorimeter, the stochastic contribution to the resolution is $0.07/\sqrt{E}$. Can we conclude that the energy resolution for an electron of energy $E = 50\,\mathrm{GeV}$ is 1%?

Discussion

Electromagnetic calorimeters are detectors that measure the kinetic energy of charged particles by exploiting one or more interaction mechanisms between charged particles and matter, including fluorescence, Cherenkov light emission, and ionisation. In general, only a fraction of the total initial energy is converted into a visible signal: the proportionality between the measured signal and the total energy allows to measure the latter, after a proper calibration is performed. Electromagnetic calorimeters can be broadly classified into two categories: *homogeneous* and *sampling*, depending on whether the active medium is composed of the same material, or interleaved with layers of inactive absorbers which degrade the energy of the incoming particle. The total energy resolution depends on the choice of active material, which determines the statistics of signal carriers per unit of deposited energy (e.g. the statistics of scintillation photons), on the signal generation and electronics (efficiency of the photodetector, electronic noise), and on other geometrical properties of the detector (e.g. uniformity, dependence of the response with the particle impact point, etc.). In most applications, the relative energy resolution can be parametrised in terms of these three contributions as:

$$\frac{\sigma(E)}{E} = \frac{a}{\sqrt{E}} \oplus \frac{b}{E} \oplus c, \tag{2.93}$$

where the symbol $\oplus$ indicates sum in quadrature. The three contributions are called *stochastic*, *noise*, and *constant term*, respectively. As a general rule, homogeneous calorimeters shine for their small stochastic term of order 1% in units of $1/\sqrt{E/\text{GeV}}$, while for sampling calorimeters the stochastic term is in the range $5 \div 20\%$, in the same units. The importance of the noise term a depends on the signal collection type: scintillation and Cherenkov calorimeters coupled to high-gain PMT suffers the least from the electronic noise, while the noise is usually larger for calorimeters that collect the signal in the form of charge (e.g. semiconductive, gas sampling, and noble-gas calorimeters), since a preamplifier is the first element in the readout chain. For this contribution to be subleading in the GeV range, the parameter b needs to be kept at the 100 MeV level per channel. For use in high-energy experiments, where particles with energies of hundreds of GeV need to be measured, the constant term ends up to be the limiting factor to the ultimate energy resolution. As an example, the electromagnetic calorimeters employed by the CMS and ATLAS experiments at the LHC are built with different technologies, but achieve similar physics performances, overall. The CMS detector makes use of a homogeneous scintillation calorimeter based on $PbWO_4$ crystals. A test beam on a small prototype yielded a stochastic term of $3.3\%/\sqrt{E/\text{GeV}}$, a noise term of $0.19/(E/\text{GeV})$, and a local constant term of 0.27%. When averaged over the full detector acceptance, the goal constant term needs to be kept below 0.5%, which is challenging since the whole detector is composed of about hundred thousand crystals that need to be inter-calibrated. This problem is somehow relieved by the ATLAS setup, which uses instead a sampling liquid-Ar calorimeter, at the price of increasing the stochastic term. A test beam on a prototype

yielded a stochastic term of $10\%/\sqrt{E/\text{GeV}}$, a noise term of $0.25/(E/\text{GeV})$, and a local constant term of 0.3%.

Solution

As discussed above, the energy resolution of an electromagnetic calorimeter depends on the energy as in Eq. (2.93). For an electron with $E = 50\,\text{GeV}$ and a calorimeter with $a = 7\%$, the stochastic term is $7\%/\sqrt{50} \approx 1\%$. The latter has to be added in quadrature to the constant and noise term to obtain the total relative energy resolution. We can estimate an upper limit to the noise and constant terms such that they do not contribute individually to the total relative resolution by more than a certain fraction f, that we can conventionally set to e.g. $f = 0.1$. With this choice:

$$\frac{\sigma(E)/E - 1\%}{1\%} < 0.1 \quad \Rightarrow \begin{cases} \frac{1}{2}\left(\frac{b/50\ \text{GeV}}{1\%}\right)^2 \lesssim 0.1, & b \lesssim 220\,\text{MeV} \\ \frac{1}{2}\left(\frac{c}{1\%}\right)^2 \lesssim 0.1, & c \lesssim 0.5\% \end{cases} \tag{2.94}$$

We can therefore conclude that the energy resolution for an electron of energy $E = 50\,\text{GeV}$ is about 1% provided that the noise and constant term are below about 200 MeV and 0.5%, respectively.

Suggested Readings

A succint but complete review of calorimetry in particle physics can be found in Ref. [20]. More informations on the state-of-the-art in calorimetry can be found in the PDG review [2] and references therein.

Bando n. 1N/R3/SUB/2005

Problem 2.34 A relativistic electron releases energy in a block of BGO, generating a signal of about 10^6 p.e./GeV, while the signal generated in a block of lead glass of the same size is only 10^3 p.e./GeV. How can such a difference be explained?

Discussion

Both BGO and lead glass feature a radiation length X_0 of about 1 cm and a critical energy of about 10 MeV [5]. An electron of few GeV energy loses energy mostly by radiation. The emitted bremsstrahlung photons undergo pair-production, with subsequent photon emission. The resulting electromagnetic shower is characterised by an energy profile

$$\frac{dE}{dt} = E_0\, b\, \frac{(b\,t)^{a-1} e^{-b\,t}}{\Gamma(a)}, \tag{2.95}$$

where $t = x/X_0$ and a and b are constants that depend on the material. Simplifying the shower development as a series of $1 \to 2$ branches ($e^{\pm} \to e^{\pm}\gamma$ and $\gamma \to e^+e^-$)

with equal energy sharing and separated by a distance X_0, so that the energy per constituent at a depth t is $E/2^t$, it follows that the total track length $L(t)$ from electrons, positrons, and photons, after traversing t radiation lengths is given by

$$L(t) = 2^t \, X_0. \tag{2.96}$$

The maximum number of radiation lengths $t_{\max}$ is determined by the condition that the electron/positron energy falls below the critical energy E_c, i.e. $t_{\max} = \ln(E/E_c)/\ln 2$, and

$$L = 2^{\frac{\ln E/E_c}{\ln 2}} \, X_0 = \left(\frac{X_0}{E_c}\right) E. \tag{2.97}$$

A more refined treatment of shower development, will still predict the total track length L to be *proportional* to the initial energy. Along their path, electrons and positrons excite the fluorescent levels of the crystal, characterised by an average excitation energy ε, so that the total photon output N_γ is still proportional to the initial energy E.

Solution

BGO, an acronym for $(Bi_2\,O_3)_2(Ge\,O_2)_3$, is a scintillating crystal. The mean excitation energy per photon is reported in Table 2.2 and is about $300\,\text{eV}/\gamma$, or $3 \times 10^6\ \gamma/\text{GeV}$, which is in the ballpark of the value reported by the problem (the ultimate p.e. statistics depends on the PMT collection and quantum efficiency). Lead glass (Pb O) is an amorphous material and does not scintillate. It has a large refraction index ($n \approx 1.8$) and is transparent to visible wavelengths, which makes it a good Cherenkov radiator. Assuming a quality factor N_0 of about $90\,\text{cm}^{-1}$, see Eq. (2.21), and a total charged track length as in Eq. (2.97), an upper limit to the number of p.e. per GeV can be estimated as:

$$\begin{aligned} \frac{N_{\text{p.e.}}}{E} = \frac{N_{\text{p.e.}}}{L}\frac{L}{E} &\approx 90\,\text{cm}^{-1}\,\langle \sin^2\theta_c\rangle \cdot (2/3)\frac{X_0}{E_c} = \\ &= 90\,\text{cm}^{-1} \cdot 0.69 \cdot (2/3)\frac{1.3\,\text{cm}}{10\,\text{MeV}} = 5 \times 10^3/\text{GeV}, \end{aligned} \tag{2.98}$$

where the factor of $2/3$ accounts for the fact that only electrons and positrons produce Cherenkov light. This estimate does not account for the fact that the simple shower model is not well representative of the energy distribution within the shower: the bremsstrahlung cross section $d\sigma/d\nu$ for emitting one photon with frequency ν is approximately proportional to ν^{-1}, see e.g. Eq. (2.68) of Ref. [1], so that the secondary e^+e^- pairs from γ conversion are preferably soft, with implications on the total Cherenkov light yield. A more accurate estimation would yield a smaller value $N_{\text{p.e.}}/E \approx 10^3/\text{GeV}$ [20].

The difference between the two materials can be therefore ascribed to the different mechanism by which photoelectrons are produced in the two materials.

Suggested Readings

The reader is addressed to Ref. [20] for a primer on calorimetry for particle physics.

Bando n. 13153/2009

Problem 2.35 Measuring the energy of hadronic particles through calorimetric methods is a fundamental ingredient in HEP experiments. When a hadron produces a shower, on average 30% of the initial energy is transformed into "invisible" energy. Indicate which mechanisms are responsible for the production of invisible energy and discuss at least one method to recover it.

Discussion

The physics of hadronic cascades is by far more involved compared to the development of electromagnetic showers due to the richness of interactions that hadronic particles undergo when crossing matter. The interaction of a high-energy hadron with a typical calorimetric material, like iron, lead, or copper, involves the production of energetic secondary hadrons through strong interactions with typical interaction lengths of about $35\,A^{1/3}\,\mathrm{g\,cm^{-2}}$, followed by the degradation of their energy by nuclear reactions that produce nuclear excitation, evaporation, spallation, fission, etc., resulting in particles with characteristic nuclear energy (100 keV ÷ a few MeV). The low energy spectrum of the hadronic cascade is dominated by neutrons, photons, electrons and positrons, the latter produced by the interaction of photons with matter. Photons are produced by two main mechanisms: from $\pi^0 \to \gamma\,\gamma$ and from nuclear de-excitations and (n, γ) reactions. The latter can come delayed up to 1 μs with respect to the primary interaction, and overall account for about 30% of the total cascade energy. Since the number of high-energy interactions that produce pions increases with energy, the fraction of energy drained away in the form of $\pi^0 \to \gamma\,\gamma$ photons increases with energy. The hadronic shower in usually initiated inside the so-called *radiator*, whereas the energy measurement is performed in the active material that samples the cascade. Both the hadronic and electromagnetic component of the cascade contribute to the energy measurement in the active material, although with different efficiencies. Let η_e (η_h) be the efficiency of detecting the energy contained in the electromagnetic (hadronic) component. The total energy measured by the interaction of a high-energy hadron with initial energy E is therefore given by:

$$E^h_{\mathrm{vis}} = [\eta_e\, F_{\pi^0}(E) + \eta_h\, F_h(E)]\, E = \eta_e \left[1 + \left(1 - \frac{\eta_h}{\eta_e}\right) F_h(E)\right] E, \qquad (2.99)$$

where $F_h = 1 - F_e$ is the hadronic energy fraction, which depends on the initial hadron energy [20]. The ratio between the response to an hadron h and to an electromagnetic particle, like an electron, is therefore:

$$\frac{E^h_{\mathrm{vis}}}{E^e_{\mathrm{vis}}} \equiv \left(\frac{e}{\pi}\right)^{-1} = 1 + \left(1 - \frac{\eta_h}{\eta_e}\right) F_h(E). \qquad (2.100)$$

Since $\eta_h \neq \eta_e$ in general, and because of the dependence of F_h with energy, Eq. (2.100) implies that

- the energy response of a hadronic calorimeter is in general non-linear;
- the energy resolution is worse than for an electromagnetic calorimeter due to the stochastic fluctuations on F_h;
- the energy response is not gaussian.

For example, in a homogeneous calorimeter, $e/\pi \approx 1.4$ as a result of the lower efficiency of detecting the hadronic component. This problem can be greatly mitigated by tuning the ratio η_h/η_e to unity, i.e. by *compensating* the calorimeter for the intrinsically different response to the hadronic component.

Solution

The origin of invisible energy in hadronic cascades can be tracked down to the production of delayed photons, soft neutrons that undergo nuclear reactions giving low-range particles, and to the production of nuclear binding energy, which is again drained away in the form of low-range nuclear decays. Although such energy is not measurable, it is possible to compensate for it in a statistical sense by decreasing the sensitivity of the detector to the electromagnetic component. For example, in a sampling calorimeter made of high-Z material like brass, uranium, or lead, interleaved with a plastic organic scintillator, the response to the electromagnetic cascade gets reduced proportionally to the sampling fraction, i.e. the fraction of active material. The latter can be tuned by varying the thickness of the scintillator layers. On the contrary, the response of the scintillator to fast neutrons is only marginally affected, since a recoil proton with $T \sim 1$ MeV has a range of a few tens of microns, see Eq. (2.35), hence it will always interact in the active material regardless of its thickness. By tuning the e/π ratio to unity, the energy resolution can be grearly enhanced.

Suggested Readings

The review article [20] gives a concise but clear discussion of the phenomenology of hadron cascades, with quantitative description of compensation in real detectors.

Bando n. 18211/2016

Problem 2.36 Which processes among pair-production, Compton scattering, and photoelectric effect, are non-negligible in the interaction of γ emitted by a ^{60}Co source with a Ge detector? Which process has necessarily to happen in order to measure the total photon energy?

Discussion

Thanks to the large Z value and the small excitation energy, see Table 2.2, Ge detectors place among the most precise detectors for γ spectroscopy below a few MeV. When dealing with γ radiation, an important property of the detector is the photopeak efficiency, i.e. the efficiency of detecting a photon which is entirely absorbed

by photoelectric effect. For Ge detectors and photons of order 1 MeV energy, the photo-peak efficiency is $\lesssim 1\%$, see e.g. Fig. 10.20 of Ref. [1].

Solution

In its β-decay chain, the ^{60}Co isotope produces two monochromatic photon lines of energy 1.17 and 1.33 MeV, hence just above the pair-production threshold $E_{\rm th} = 2m_e \approx 1.02$ MeV. The K-shell for Ge is located at 11 keV [9], hence the photoelectric effect is expected to be small for the ^{60}Co photons, while Compton scattering should be the dominant interaction mechanism. Indeed, from Ref. [6], we find $\sigma_{\rm p.e.} \approx 5 \times 10^{-2}$ barn, $\sigma_{\rm Comp} \approx 6$ barn, and $\sigma_{\rm pair} \approx 10^{-2}$ barn for $E_\gamma = 1.25$ MeV. If the photon undergoes Compton scattering, only the energy deposited by the recoil electron can be measured by the detector. The interaction length for photons in Ge is given by:

$$\lambda_{\rm Comp} = (n\,\sigma_{\rm Comp})^{-1} = \left(\frac{5.3\,{\rm g\,cm^{-3}} \cdot 6 \times 10^{23}\,{\rm mol^{-1}}}{72\,{\rm g\,mol^{-1}}} \cdot 6\,{\rm barn}\right)^{-1} \approx 4\,{\rm cm}, \tag{2.101}$$

so there is a finite probability that the photon undergoes one Compton scattering only before leaving the active volume, if the latter is a a few mm thick, like in practical Ge detectors. The maximum electron recoil energy is given by Eq. (1.139), namely:

$$T_{\rm max} = E_\gamma \frac{2\,k}{1+2\,k} = 0.96,\ 1.1\,{\rm MeV}, \tag{2.102}$$

where $k = E_\gamma/m_e$. For example, the range in Ge for an electron of kinetic energy 1.1 MeV is about 1.2 mm [5], hence there is a non-negligible chance that the recoil electron escapes the active volume. The same holds for the photoelectrons, which have energies $E_\gamma - \mathscr{B} \approx 1.16$ and 1.32 MeV, and ranges below 2 mm.

The only reactions that guarantee a full energy measurement are therefore the photoelectric effect (probability $\approx$1%), with full electron confinement, and pair-production (probability $\approx 0.2\%$). In the latter case, the emitted $e^\pm$ have an energy of about $(E_\gamma - 2m_e)/2 \approx 75$ and 150 keV and ranges of about 25 and 85 μm, respectively, and are therefore very likely to be fully contained in the active volume. After annihilation with an atomic electron, the $2m_e$ rest energy of the e^+e^- pair restores the full energy measurement if the two photons from positronium annihilation interact with the active material (the interaction length for 0.5 MeV photons is about 2.4 cm).

Bando n. 18211/2016

Problem 2.37 Estimate the contribution to the energy resolution (FWHM) due to the stochastic fluctuations in silicon calorimeters generated by photons of energy 2 keV, 6 keV, and 15 keV.

Discussion

If the measured energy E is distributed according to a Gaussian law with mean $\mu = 0$ and standard deviation σ, the FWHM resolution is defined as the interval such that the p.d.f equals half of its value at the mean position μ, i.e.:

$$\mathcal{N}(x_{\pm};\ \mu, \sigma) = \frac{1}{2}\mathcal{N}(0;\ \mu, \sigma) \quad \Rightarrow \quad x_{\pm} = \pm\sqrt{2\ln 2}\,\sigma \approx \pm 1.177\,\sigma$$
$$\sigma_{\text{FWHM}} = (x_{+} - x_{-}) = 2.35\,\sigma \qquad (2.103)$$

When dealing with energy resolution with particle detectors, an important concept is the so-called *Fano factor* (F). If a particle produces on average $N = E/\varepsilon$ signal carriers through independent random interactions characterised by probability p, the stochastic fluctuation in this number is $\sqrt{N}$ from Poisson statistics, and the relative energy resolution is $1/\sqrt{N}$. However, if the detector cannot but absorb all of the particle energy by converting it into detectable signal carriers, the multiplicity of the latter is ideally fixed to N and there would be no stochastic fluctuations at all. This is seldom the case, since there is in general a partioning of the energy transferred by the particle to the active material into more channels, some of which may not produce signal carriers. Indeed, in some circumstances it is observed that the relative energy variance is smaller than the Poisson expectation by an empirical factor F, with $F < 1$, i.e.:

$$\frac{\sigma}{E} = \sqrt{\frac{F\,\varepsilon}{E}} \qquad (2.104)$$

Semiconductors that absorb the full particle energy into eh-pairs, feature a Fano factor of about 0.12. The Fano factor for ionisation detectors has been discussed in Problem 2.8. More informations can be found in Chap. 4 of Ref. [7].

Solution

At energies below 15 keV, the photoelectric effect dominates the interaction of photons with silicon, see e.g. Ref. [6]. We can therefore assume that the photon interacts with one atom by emitting an electron of a few keV energy. The photo-produced electron loses energy by collision loss and creates additional electon-hole pairs along its track. At $E = 2$ keV, the photoelectron will most likely originate from a K-shell emission. Since the K-edge in silicon is at 1839 eV [9], the resulting photo-electron will be rather soft as for Eq. (2.23). However, the ionised atom is in an excited state, which will bring to the emission of either K-α and K-β photons, which undergo photoelectric effect from L-shells with the emission of secondary photoelectrons, or to the emission of short-range Auger electrons [5]. In any case, the secondary particles will release energy in the active medium, so that one can still assume that the whole photon energy is absorbed with little energy partitioning. This reduces the standard deviation of the number of electron-hole pairs N_{eh} from the Poisson expectation of $1/\sqrt{N_{eh}}$ to $\sqrt{F/N_{eh}}$, with $F \approx 0.12$ for silicon. The mean excitation

energy is $\varepsilon = 3.6\,\text{eV}$, see Table 2.2. We can therefore estimate the FWHM of the measured signal to be:

$$\sigma_{\text{FWHM}} = 2.35\sqrt{\frac{F\varepsilon}{E}} = 2.35\sqrt{\frac{0.12 \cdot 3.6\,\text{eV}}{E}} = \begin{cases} 3.4\% & E = 2\,\text{keV} \\ 2.0\% & E = 6\,\text{keV} \\ 1.3\% & E = 15\,\text{keV} \end{cases} \tag{2.105}$$

Suggested Readings

Reference [21] discusses in more detail the use of silicon detectors for γ spectroscopy, with examples of measured spectra from nuclear candles. A broader discussion on the phenomenology of photoelectric absorption in matter can be found in Ref. [7].

Bando n. 1N/R3/SUB/2005

Problem 2.38 A piece of Na I (Tl) scintillator, read-out by a phototube, is used to measure the ^{137}Cs line: estimate the energy resolution by listing the contributing factors.

Solution

The energy resolution for a coupled scintillator-phototube detector is described by Eq. (2.45). The ^{137}Cs isotope produces a monochromatic X-ray emission with energy $E = 661\,\text{keV}$. The main contribution to the energy resolution comes from the statistics of photoelectrons, which depends on the mean number of photons $n_\gamma = E/\varepsilon$, where ε is the mean excitation energy, see Table 2.2, and on the overall efficiency of the photocathode. The electronic noise plays also an important role. An other contribution may come from the dependence of the response with the photon impact point and from an imperfect shower containment. Assuming $\varepsilon_Q\,\varepsilon_C = 0.2$ for a typical PMT, see e.g. Table 34.2 of Ref. [2], and negligible noise from the electronics and amplification statistics ($f_N = 1$, $G \gg 1$), the relative energy resolution (FWHM) can be estimated to be:

$$\frac{\sigma_{\text{FWHM}}}{E} = 2.35\sqrt{\frac{\varepsilon}{E \cdot \varepsilon_Q \varepsilon_C}} = 2.35\sqrt{\frac{22\,\text{eV}}{661\,\text{keV} \cdot 0.2}} = 3.0\%, \tag{2.106}$$

see Problem 2.37. No Fano factor has been accounted for in Eq. (2.106), since there is no evidence for its presence in scintillators.

Bando n. 5N/R3/TEC/2005

Problem 2.39 Estimate the energy resolution at 140 keV of a photo-detector equipped with Na I (Tl) crystals.

Solution

We can refer to Problem 2.38 for determining the energy resolution of a similar setup. Assuming $\varepsilon_Q\,\varepsilon_C = 0.2$ for a typical PMT and negligible noise from the electronics and amplification statistics, the relative energy resolution (FWHM) can be estimated to be:

$$\frac{\sigma_{\text{FWHM}}}{E} = 2.35\sqrt{\frac{\varepsilon}{E\cdot\varepsilon_Q\,\varepsilon_C}} = 2.35\sqrt{\frac{22\,\text{eV}}{140\,\text{keV}\cdot 0.2}} = 6.6\%, \tag{2.107}$$

where $\varepsilon = 22\,\text{eV}$ is the mean excitation energy for Na I (Tl), see Table 2.2. See Problem 2.37 for the definition of FWHM.

Bando n. 18211/2016

Problem 2.40 A scintillator emits $10^4\ \gamma$/MeV. Calculate the resolution (FWHM) for a 4 MeV particle assuming a total light collection efficiency $\varepsilon_C\,\varepsilon_Q$=1.

Solution

The energy resolution of the detector is described by Eq. (2.45). Assuming $\varepsilon_Q\,\varepsilon_C = 1$ and negligible noise from the electronics and amplification statistics, the relative energy resolution (FWHM) can be estimated to be:

$$\frac{\sigma_{\text{FWHM}}}{E} = 2.35\sqrt{\frac{\varepsilon}{E}} = 2.35\sqrt{\frac{10^{-4}\,\text{MeV}}{4\,\text{MeV}}} = 1.2\%. \tag{2.108}$$

See Problem 2.37 for the definition of FWHM.

Bando n. 13153/2009

Problem 2.41 Calculate the energy resolution for photons of energy E measured by a solid state detector with ionisation energy ε, leakage current I_d, and integration time of the associated electronics equal to T_S.

Solution

If the photon energy is intirely absorbed by the detector, the mean signal charge Q collected at the electrodes of the p-n junction and its standard deviation are given respectively by:

$$Q = \frac{E}{\varepsilon}\,e, \qquad \sigma_Q = \sqrt{\frac{F\,E}{\varepsilon}}\,e, \tag{2.109}$$

where $F \approx 0.12$ is the Fano factor in silicon. In the integration time T_S taken by the electronics to shape the signal, the leakage current contributes to the noise via an equivalent squared-charge:

$$Q_n^2 = 2\, e\, I_d\, T_S, \tag{2.110}$$

see e.g. Sect. 34.8 of Ref. [2]. Since the noise from the leakage current and the statistical fluctuation in the number of signal carriers are uncorrelated, the relative energy resolution is given by the sum in quadrature:

$$\frac{\sigma_E}{E} = \frac{\sqrt{\sigma_Q^2 + Q_n^2}}{Q} = \sqrt{\frac{\varepsilon}{E}} \sqrt{F + \left(\frac{2\, I_d\, T_S}{e}\right) \frac{\varepsilon}{E}} \tag{2.111}$$

Suggested Readings

For a concise overview of low-noise front-end electronics for particle detectors, the reader is addressed to Sect. 34.8 of Ref. [2].

Bando n. 1N/R3/SUB/2005

Problem 2.42 The drift velocity of electrons in some gas mixture is $v = 5\,\text{cm}/\mu\text{s}$. What does it imply for a multiwire chamber with wire spacing $s = 2\,\text{mm}$, and what for a drfit chamber read-out by a TDC with 500 MHz clock?

Discussion

Multiwire chambers have been briefly discussed in Problem 2.52. Drift tubes (DT) are gaseous ionisation detectors that measure the time taken by the primary ionisation electrons to drift from their point of formation up to the anode. For ions moving in a gas, the drift velocity v is roughly proportional to the electric field intensity:

$$v = \mu\, E, \tag{2.112}$$

where μ is called mobility and depends on the pressure P and temperature T of the gas, while it is almost independent of the electric field. Electrons can instead reach much higher velocities compared to ions, and the mobility μ depends on E in such a way that a saturation of the velocity at values of order 50 μm/ns is reached for $E \sim 1\,\text{kV/cm}$ at STP. By making the electric field as uniform as possible in the drift region, Eq. 2.112 implies a proportionality between the distance from the anode of the primary ionisation position and the drift time. The latter is defined as the time interval between a fast trigger, that provides the start time to the clock, and the time of formation of the electric signal at the anode. Drift tubes are built according to this concept. Typical position resolutions achievable with DT are 100 μm over few drift lengths d of a few cm. The position resolution is determined by the sum in quadrature

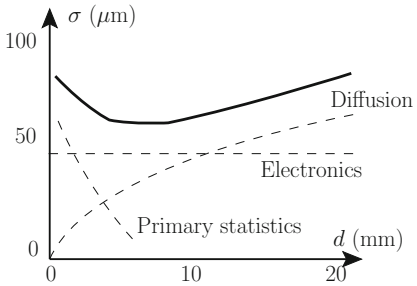

Fig. 2.10 Typical position resolutions in a drift chamber as a function of the drift length d. The total resolution is broken up into three main contributions: statistics of the primary ionisation, noise from the electronics, and charge diffusion

of three dominant contributions: the statistics of primary ionisation (relevant at small d), the electronic noise (independent from d), and electron diffusion (proportional to $\sqrt{d}$). Figure 2.10 provides a qualitative description of the position resolution as a function of the drift length d.

Solution

A MWPC with wire spacing $s = 2\,\text{mm}$, has a spatial resolution along the coordinate y orthogonal to the wires:

$$\sigma_y^{\text{MW}} = \frac{s}{\sqrt{12}} = \frac{2\,\text{mm}}{\sqrt{12}} \approx 580\,\mu\text{m}. \tag{2.113}$$

The factor $\sqrt{12}$ accounts for the fact that the particles arrive at the detector uniformly distributed across y. The time resolution is therefore given by

$$\sigma_t^{\text{MW}} = \frac{\sigma_y^{\text{MW}}/2}{v} = \frac{580\,\mu\text{m}/2}{5\,\text{cm}/\mu\text{s}} \approx 5.8\,\text{ns} \tag{2.114}$$

In Eq. (2.114), the factor of $1/2$ at the numerators comes from the fact that a primary ionisation generated outside of the $\pm s/2$ range from a given wire will be detected by one of the two neighbouring wires. For a DT readout by a time-to-digital converter (TDC), the TDC clock period f^{-1} sets a minimum time resolution

$$\sigma_t^{\text{DT}} = \frac{f^{-1}}{\sqrt{12}} = \frac{2\,\text{ns}}{\sqrt{12}} = 0.58\,\text{ns}. \tag{2.115}$$

Again, one has to divide by $\sqrt{12}$ since the actual arrival time at the anode is uniformly distributed across the time interval f^{-1} between subsequent clocks. The position uncertainty induced by the TDC clock is therefore given by:

$$\sigma_{y,\,\text{clock}}^{\text{DT}} = \sigma_t^{\text{DT}} \cdot v = 0.58\,\text{ns} \cdot 5\,\text{cm}/\mu\text{s} \approx 29\,\mu\text{m}. \tag{2.116}$$

This term contributes to the electronic noise shown in Fig. 2.10. The overall position resolution depends however on other factors, as discussed above. Typical position resolutions of a conventional DT is about 100 μm, which is anyway smaller than the one from a typical MWPC.

Suggested Readings

For a comprehensive review of DT, the reader is addressed to Ref. [22].

Bando n. 1N/R3/SUB/2005

Problem 2.43 A depleted microstrip silicon detector has a strip pitch of 50 μm and operates without charge division. What is its spatial resolution?

Discussion

A *silicon microstrip* is a solid-state detector consisting of a wafer of doped silicon, for example, of a high-resistivity n-type with typical thickness of about 300 μm, with p-n junctions shaped in the form of long and thin parallel strips separated by a distance (pitch) ranging between 20 and 200 μm. In a possible setup, one surface of the wafer is grounded and the strips are implanted on the opposite side and connected to the bias voltage via DC or AC coupling. The junction may be realised by p^+-type silicon and, for a typical wafer thickness, it gets completely depleted by a bias voltage of order 100 V. A MIP loses $1.66 \cdot 2.33\,\text{MeV/cm} \approx 3.87\,\text{MeV/cm}$ in silicon [5]. Given that the average excitation energy is $\varepsilon = 3.6\,\text{eV}$, a total of 3×10^4 eh-pairs are produced on average across a 300 μm-thick junction. The signal carriers drift under the effect of the bias voltage and the induced charge is measured by the front-end electronics.

The *charge division* method consists in an analog measurement of the signal from the strips close to the one which recorded the hit, i.e. the one with the largest signal yield. The centre-of-mass of the strip charges $\bar{x} = \sum_i Q_i\, x_i / \sum_i Q_i$, where i runs over the strips and x_i (Q_i) are the strip positions (measured signal), provides an estimator of the impact position with typical resolution of about

$$\sigma_x^{\text{ana}} \sim \frac{d}{\text{SNR}}, \tag{2.117}$$

where d is the strip pitch and SNR is the signal-over-noise ratio. This can be easily proved by using the standard propagation of error for uncorrelated measurements, see Eq. (4.73):

$$\bar{x} = \frac{\sum_i Q_i\, x_i}{\sum_i Q_i} \quad \Rightarrow \quad \sigma_{\bar{x}}^2 = \sum_j \left| \frac{\partial \bar{x}}{\partial Q_j} \right|^2 \delta Q_j^2 = \sum_j \frac{\left(x_j - \bar{x}\right)^2}{\left(\sum_i Q_i\right)^2} \delta Q_j^2 = d^2 \frac{\sum_j \delta Q_j^2}{\left(\sum_j Q_j\right)^2},$$

$$\sigma_{\bar{x}} = \frac{d}{\text{SNR}}, \quad \text{with} \quad \text{SNR} = \frac{\sum_j Q_j}{\sqrt{\sum_j \delta Q_j^2}} \equiv \frac{S}{N}. \tag{2.118}$$

Conversely, if the strips can be read in digital mode only, the position resolution is given by the strip pitch:

$$\sigma_x^{\text{dig}} = \frac{d}{\sqrt{12}}, \tag{2.119}$$

Additional sources of uncertainty affecting the collection of charge carriers, like thermal diffusion, multiple-scattering, δ-rays, should be also considered for realistic detectors.

Solution

In the absence of charge division, the spatial resolution of a microstrip detector is primarily determined by the pitch size d. Since the particle flux can be asumed to be uniformly distributed across the microstrip detectors, we can estimate the spatial resolution (FWHM) as:

$$\sigma_{\text{FWHM}}^x = 2.35\frac{d}{\sqrt{12}} = 34\ \mu\text{m}, \tag{2.120}$$

where the factor of $1/\sqrt{12}$ comes from the assumed flux uniformity, see Problem 2.42.

Suggested Readings

For a first introduction to microstrip detectors, the reader is addressed to Sect. 10.6 of Ref. [1].

Bando n. 18211/2016

Problem 2.44 A silicon detector is made of a pixels with dimension 100 μm $\times$ 200 μm. What is the smallest spatial resolution in the two dimensions, if the detector has digital readout?

Discussion

Pixel detectors are semiconductive detectors where the active volume is segmented in small picture elements (pixels), which are independently read-out. Planar pixel detectors are commonly employed in HEP experiments as vertex detectors, thanks to their superior spatial resolutions in two dimensions, which allows for a small occupancy even at the closest distance to the interaction point, and their close-to-ideal efficiency to detect the passage of ionising particles.

Solution

If the detector is operated in digital readout, see Problem 2.43, a lower bound to the spatial resolution (FWHM) in the two directions is given by:

$$\begin{cases} \sigma^x_{\text{FWHM}} = 2.35\,\frac{d_x}{\sqrt{12}} = 68\ \mu\text{m} \\ \sigma^y_{\text{FWHM}} = 2.35\,\frac{d_y}{\sqrt{12}} = 136\ \mu\text{m} \end{cases} \tag{2.121}$$

where the factor of $1/\sqrt{12}$ comes from the assumed flux uniformity, see Problem 2.42.

Suggested Readings

For a comprehesive introduction to pixel detectors in HEP experiments, the reader is addressed to Ref. [21].

Bando n. 18211/2016

Problem 2.45 Why is a diode used as radiation detector usually operated with an inverse bias?

Solution

A p-n junction operated at inverse bias give rise to an active region depleted from mobile charge where an intense electric field can sweep out free charges liberated by a ionising particle. The thickness of the depletion zone for the case of a silicon *p-n* junction realised by a p^+-doped material put into contact with a lightly doped n region, is approximately given by:

$$W = 0.5\sqrt{\left(\frac{\rho_{\text{n}}}{\Omega\ \text{cm}}\right)\left(\frac{V_0 + V_{\text{bias}}}{\text{V}}\right)}\ \mu\text{m}, \tag{2.122}$$

where ρ_{n} is the resistivity of the *n*-type region, $V_0 \sim 1$ V is the barrier voltage, and V_{bias} is the bias voltage, see e.g. Ref. [2]. The importance of applying an inverse bias to the junction as to enlarge the active volume is made clear by Eq. (2.122). For example, for typical values $\rho_{\text{n}} = 2 \times 10^4\ \Omega$ cm, the thickness of the depletion region would change from 70 to 700 μm, if a reverse bias $V_{\text{bias}} = 100$ V is applied.

Suggested Readings

An introduction to the physics of semiconductors for particle detectors can be found in Chap. 20 of Ref. [1].

Bando n. 13705/2010

Problem 2.46 Consider a D^0 meson produced with an energy of 20 GeV. Determine the spatial resolution necessary to measure the production and decay vertex position, and indicate which detectors are best suited for an efficiency exceeding 90%.

Solution

The D^0 meson decays via the electroweak interaction with a lifetime of about 0.41 ps, corresponding to $c\tau \approx 120\ \mu\text{m}$ [2]. A good channel to reconstruct its decay is $D^0 \to K^{\pm}\pi^{\mp}$. The probability of surviving up to a distance d ot more from its production vertex is given by Eq. (1.174):

$$\text{P}\left[x \geq d\right] = \exp\left[-\frac{mc}{|\mathbf{p}|}\frac{d}{c\tau}\right] = \exp\left[-\frac{1}{\sqrt{\gamma^2-1}}\frac{d}{c\tau}\right] \tag{2.123}$$

Requiring this probability to be at least 90% is equivalent to impose that the flight distance should be in excess of:

$$d_{90\%} = (-\ln 0.9)\, c\,\tau\,\gamma = (0.105 \cdot 123 \cdot 11)\ \mu\text{m} \approx 140\ \mu\text{m}, \tag{2.124}$$

where we have used the fact that $\gamma \approx 11$ is large. Therefore, if we want to reconstruct at least 90% of the D^0 decays from their decay vertex, the vertex resolution must be smaller than about 140 μm. This can be easily achieved by silicon-based vertex detectors, either pixel- or mictrostrip-based.

Discussion

For $E = 20\,\text{GeV}$, the decay products have energy of about 10 GeV each. In this regime, multiple scattering usually dominates the tracking resolution when using silicon detectors with pixel/pitch size $\lesssim 100\ \mu\text{m}$, see Problem 3.9. The *impact point resolution* (σ_{ip}) is the uncertainty on the position of closest approach of the track extrapolation to the primary vertex point (PV), and is related to the resolution on the position of the secondary vertex (SV), see Fig. 2.11. Modulo resolution effects, the quantity

$$s^j_{\text{ip}} = \text{sign}\left[\mathbf{ip}_j \cdot (\mathbf{SV} - \mathbf{PV})\right] \tag{2.125}$$

should be positive for tracks emerging from the same secondary vertex. Conversely, the detector rsolution smears the impact point of tracks emerging from the PV around zero, with equally likely values of s_{ip}. This property can be exploited to define tagging algorithms for displaced vertexes and experimental methods to measure their efficiency in data [24, 25]. Assuming a MS-dominated regime, the impact point resolution is given by:

$$\sigma_{\text{ip}} \approx r_1\sqrt{\langle\theta_1^2\rangle}, \tag{2.126}$$

where r_1 is the distance of the innermost silicon layer from the interaction point and $\langle\theta_1^2\rangle$ is given by Eq. (2.8). For example, assuming the design of the CMS pixel detector, one has $r_1 = 4.4\,\text{cm}$ and a MS mean angle of about 2×10^{-4} rad at $|\mathbf{p}| = 10\,\text{GeV}$, giving $\sigma_{\text{ip}} \approx 10\ \mu\text{m}$, see Ref. [26]. A more realistic simulation, which

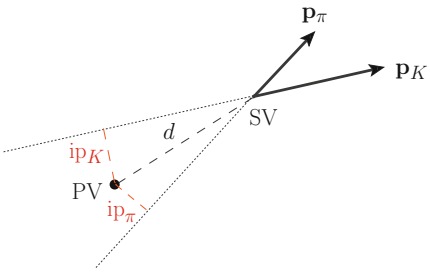

Fig. 2.11 Cartoon illustrating the two-body decay of a D^0 meson. The distance of closest approach of the extrapolation of the daughter particles trajectories to the primary vertex (PV) is called *impact parameter*

includes measurement uncertainty and MS in the beam pipe, gives about a factor of 2 larger resolution, which still satisfies the constraint of Eq. (2.124).

Suggested Readings

For an overview of tracking and vertexing performances at the LHC, the reader is recommended to read the review article [26].

Bando n. 18211/2016

Problem 2.47 Explain why Ge sensors need to be cooled, while Si sensors do not.

Solution

Germanium detectors are commonly operated at liquid nitrogen temperature ($T = 77\,\mathrm{K}$) to reduce the leakage current I_d due to thermal excitation, and hence the electronic noise and power consumption, see Problem 2.41). The bias current depends exponentially on the temperature T:

$$I_\mathrm{d}(T) \propto T^2 \exp\left[-\frac{E_\mathrm{gap}}{2\,k_\mathrm{B}\,T}\right] \quad \Rightarrow \quad \frac{I_\mathrm{d}(T_2)}{I_\mathrm{d}(T_1)} = \left(\frac{T_2}{T_1}\right)^2 \exp\left[-\frac{E_\mathrm{gap}}{2\,k_\mathrm{B}}\left(\frac{1}{T_2}-\frac{1}{T_1}\right)\right], \tag{2.127}$$

where E_gap is the energy gap, see e.g. Sect. 34.7 of Ref. [2]. Although the same effect exists in silicon, the energy gap in the latter is larger than in germanium. For example, at room temperature, one has $E_\mathrm{gap} = 1.1\,\mathrm{eV}$ for silicon and $0.7\,\mathrm{eV}$ for germanium, corresponding to a factor of 3×10^3 larger leakage current for the latter.

Bando n. 18211/2016

Problem 2.48 Which property of a SiPM makes it a preferable solution cimpared to a conventional PMT for an integrated imaging PET-MRI system?

Discussion

Silicon photomultipliers (SiPM), also known as *Pixelized Photon Detectors* (PPD) are photodetectors composed by an array of pixel-size photodiodes with typical size ranging from $25 \times 25\ \mu m^2$ to $100 \times 100\ \mu m^2$, packed over a small area, typically from $0.5 \times 0.5\,mm^2$ to $5 \times 5\,mm^2$, and operated in Geiger mode, i.e. with a bias voltage in excess of the break-down voltage. When a eh-pair is created in the depleted region, the intense electric field triggers the formation of an avalanche. The high bias voltage provides large gains per incident photon and per pixel, but proportionality between the number of photons impinging on a given cell and the collected charge is lost. The proportionality with the total input photons is restored by summing the binary cell outputs from the full array.

Solution

SiPM's represent a convenient alternative to PMT's for applications in environment with intense magnetic field, like in *positron emission tomography-magnetic resonance imaging* (PET-MRI) applications, since the amplification stage in a SiPM does not require the photoelectrons to be accelerated along the dynode of conventional PMT's, which suffers from the presence of magnetic fields, for example by altering the gain.

Suggested Readings

For an introduction to SiPM's, the reader is addressed to the dedicated PDG review [2] and references therein.

Bando n. 1N/R3/SUB/2005

Problem 2.49 Order the following detectors by decreasing dead time: silicon, plastic scintillator, drift chamber. Which one would you chose for a time measurement with resolution of a few hundred ps?

Discussion

The *dead time* τ is the time required by a detector to process one event and be ready to accept a new event. Depending whether the detector is sensitive or not to a new event while processing the previous one, two types of dead-time exist: *extendable* or *not-extendable*. In the first case, if we assume that the first event occurred at time t_0, the arrival of a new event at a time $t_1 < t_0 + \tau$ shifts the time at which the detector is ready to accept and process a new event to at least $t_2 = t_1 + \tau$. In the second case, the new event does not change the detector state at all, and the subsequent event can be accepted and processed at any time $t_1 \geq t_0 + \tau$, regardless of what happens meanwhile. See Problem 3.38 for more details.

Solution

Plastic scintillators are generally faster than inorganic scintillators, with decay times of a few ns, see e.g. Table 7.1 of Ref. [1]. Fast photodetectors can also have risetimes

below 1 ns, see e.g. Ref. [2]. A coupled scintillator-photodetector system is ready to accept and process a new event after the fluorescent excitation from the previous event have decayed to the ground level, which can take about 10 ns for fast scintillators.

A silicon strip or pixel detector has time resolutions of a few ns, but the time needed to collect the full charge released in the depleted zone can take a few tens of nanoseconds (10 ns for electrons and 25 ns for holes in a 300 μm thich detector, see Sect. 34.7 of Ref. [2]). The readout electronics further increases the processing time to at least 50 ns.

In a drift chamber, the dead time is mostly due to the time taken by the primary ionisation electrons (ions) to drift to the anode (cathode), see Problem 2.42. For a typical electron velocity of 5 cm/μs, the time needed to drift over 1 cm is about 200 ns. During this time, a new event would cause pile-up and confusion on the time measurement.

A time measurement with a few hundreds ps time resolution is best accommodated with plastic scintillators coupled to fast photo multipliers, like microchannel plate (MCP) or gas electron multipliers (GEM), with a fast sampling frequency of the readout electronics as to allow for the full pulse shape reconstruction.

Suggested Readings

More details on the dead time of particle detectors, including techniques for measuring it in the laboratory, can be found in Sect. 5.7 of Ref. [1]. Table 34.1 of Ref. [2] summarises the typical resolutions and dead times of common charged particle detectors.

Bando n. 18211/2016

Problem 2.50 The mean counting rate on single electrode for a given detector is 150 kHz. Estimate an upper bound to the processing time of the analog pre-amplifier and shaper, if the pile-up probability has to be maintained below 3%.

Solution

For what concerns the pileup of multiple events, we can use the same line of thought used to relate the true and measured rate in a non-paralyzable system, see Problems. 2.49 and 3.38. Referring to Eq. (3.186) with $\varepsilon = 1$, we can therefore invert the equation and express the true rate ν as a function of the measured rate m and of the dead time τ, i.e.

$$\nu = \frac{m}{1 - m\,\tau}. \tag{2.128}$$

Requiring that the pile-up is less than $\delta = 3\%$ amounts to require that the ratio between the measured rate and the true rate is larger than $1 - \delta$, or equivalently:

$$\frac{m}{\nu} = 1 - m\,\tau > 1 - \delta \quad \Rightarrow \quad \tau < \frac{\delta}{m} = \frac{0.03}{1.5 \times 10^5\,\text{Hz}} = 200\,\text{ns}. \tag{2.129}$$

Bando n. 18211/2016

Problem 2.51 A proportional cylindrical tube has inner radius R, wire radius r, and anodic tension V_0. What is the value of the electric field at a distance $d \leq R$ from the anode?

Solution

Let's assume that the anode is connected to a potential $V_0 > 0$ and that the cathode is grounded. The wire acquires a charge with uniform linear density. By using the cylindrical symmetry of this configuration, it is easy to prove that the electric field must be radial, i.e. $\mathbf{E} = E(d)\,\mathbf{e}_r$. By virtue of Gauss law, the field intensity $E(r)$ must scale as d^{-1}, i.e.

$$E(d) = \frac{c_0}{d}, \tag{2.130}$$

where c_0 is a constant that depends on the boundary conditions. Since $E = -\nabla V$, the electric potential $V(d)$ must be proportional to $\ln d$. Together with the boundary conditions at the two electrodes, this fully determines the potential to be:

$$V(d) = \frac{V_0}{\ln(r/R)} \ln(d/R), \tag{2.131}$$

from which we get the result:

$$E(d) = -\frac{\partial V}{\partial d} = \frac{V_0}{\ln(R/r)} \frac{1}{d}. \tag{2.132}$$

Discussion

The d^{-1} scaling of the electric field makes the cylindrical tube suitable for charge multiplication. For example, assuming typical values $r = 20\,\mu\text{m}$, $R = 5\,\text{cm}$, $V_0 = 2\,\text{kV}$, the electric field at a distance of $100\,\mu\text{m}$ from the wire is about $20\,\text{kV/cm}$, which is enough to trigger the formation of an avalanche with its resulting charge multiplication. As an eample, the gas multiplication factor M for a cylindrical chamber filled with P-10 gas (90% Ar, 10% $C H_4$) at STP can be estimated from *Diethorn* formula:

$$\ln M = \frac{V_0}{\ln(R/r)} \frac{\ln 2}{\Delta V} \ln\left(\frac{V_0}{p\,r\,\ln(R/r)\,K}\right) \approx 7.3 \quad \Rightarrow \quad M = 1.5 \times 10^3, \tag{2.133}$$

where p is the gas pressure and K and ΔV are gas-specific parameters, see e.g. Table 6.1 of Ref. [7] for a few examples.

Suggested Readings

An introduction to the physics of electronic avalanches in gas can be found in Ref. [1, 7]. For a more comprehensive review of gaseous detectors, the reader is addressed to Ref. [8].

Bando n. 1N/R3/SUB/2005

Problem 2.52 The cathode readout can be used in wire detectors, like multiwire chambers, TPC, LST, and even RPC. What does it mean? What are the main advantages of this setup?

Discussion

Multiwire proportional chambers (MWPC), time projection chambers (TPC), limited streamer tubes (LST), and resistive plate chambers (RPC) are all examples of gaseous ionisation detectors that measure the ionisation charge left behind by particles interacting with the gas. A gaseous detector consists in a pair of electrodes kept at different electrostatic potentials and separated by a gaseous medium. The anode is usually shaped in a way as to produce intense electric fields nearby its surface. A metallic wire kept at a positive voltage bias is the solution at the basis of the MWPC, TPC, and LST technology. A plane capacitor with small inter-plane distance is an other option, which is e.g. used in RPC detectors. The cathode confines the electric field and shields the detector from the outside. The usual way of opertaing a gaseous detector is to ground the cathode and read the anode in AC-coupling, i.e. separating the bias voltage from the readout electronics by means of a capacitor, see Problem 2.53. Alternatively, one can set the cathode at a negative bias voltage, and couple the anode directly to the readout electronics.

Solution

Let's consider the case where the anode consists in a set of parallel wire with small inter-distance, stretched along the coordinate x, and let y be the orthogonal coordinate. The passage of a ionising particle induces the formation of an electron avalanche in the neighbourhood of the anode. The positive ions drift towards the cathode inducing a signal (a time-dependent voltage pulse) between the two electrodes. If the detector is operated in anode readout, only the y coordinate can be measured with good resolution. If the cathode is segmented along y, like in the form of parallel strips, then a cathode readout, i.e. a measurement of the pulse induced at the cathode, offers the possibility of measuring also the x coordinate. If the cathode readout is analogic, a centre-of-gravity method allows to measure the x position with high precision (indeed, only limited by the noise of the electronics). If the readout is digital-only, the x resolution is instead determined by the granularity of the cathode.

Suggested Readings

An introduction to gaseous detectors and to their readout can be found in Sect. 6.6 of Ref. [1]. A more advanced and complete reference on the subject is provided by

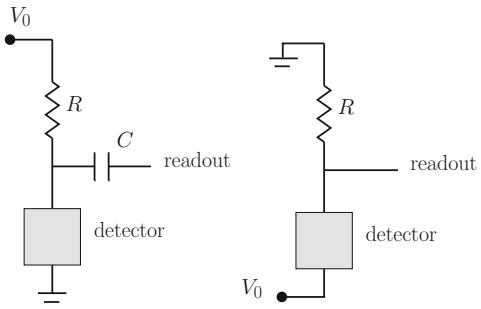

Fig. 2.12 AC and DC couplings for a generic detector

Ref. [8]. A stimulating discussion on this subject can be also found in the Nobel lecture by G. Charpak (1992), the inventor of the MWPC.

Bando n. 18211/2016

Problem 2.53 Does a radiation detector AC-coupled to its electronics have a larger noise compared to a DC-coupled detector with the same electronics?

Discussion

The readout electrode of a charge-sensitive detector, like a microstrip silicon detector, an RPC, a MWPC, etc., can be either set to a large bias voltage or be grounded. In the former case, the front-end electronics, which usually starts with a pre-amplifier, needs to be decoupled from the bias voltage by a capacitance (*AC-coupling*). In the latter case, the electrode can be directly accessed by the pre-amplifier (*DC-coupling*), see Fig. 2.12.

Solution

AC-coupling offers the advantage of having the opposite electrode (e.g. the cathode, for wire detectors) grounded, resulting in a convenient configuration to insulate the detector. However, it provides an extra decoupling capacitance in input to the readout chain, thus increasing the electronic noise compared to a DC-coupling. Indeed, for a capacitive sensor, the charge-equivalent noise Q_n can be parametrised as:

$$Q_n^2 = i_n^2 \, F_i \, T_\mathrm{S} + \left(\frac{e_n^2 \, F_v}{T_\mathrm{S}} + F_{vf} \, A_f \right) C^2, \tag{2.134}$$

where C is the sum of all capacitances shunting the input, i_n^2 and e_n^2 are the quadratic current and voltage noise densities, T_S is the characteristic shaping time, and $F_{i,v,vf}$ are devise-specific constants [2].

Suggested Readings

For an introductory discussion on the readout of silicon detectors, the reader is addressed to Sect. 10.9 of Ref. [1]. More details on low-noise electronics for capacitive detectors can be found in the dedicated PDG review [2].

Bando n. 1N/R3/SUB/2005

Problem 2.54 A discriminator is operated with a threshold $V_{\rm th} = 0.4\,\mathrm{V}$ and receives in input signals that have a constant rise-time equal to $T_{\rm S} = 10\,\mathrm{ns}$, but an amplitude variation between $V_{\rm min} = 0.5\,\mathrm{V}$ and $V_{\rm max} = 1\,\mathrm{V}$. Estimate the lower bound on the time resolution due to the variable amplitude. Which technique would you use to reduce such an effect?

Discussion

A *discriminator* is a device that produces a digital signal when an analogical input pulse overcomes a predefined threshold. A discriminator in combination with a TDC device can be used for timing measurements of signals. When the input signals differ in amplitude and/or rise-times, the time measurement performed by a discriminator with fixed threshold is affected by event-by-event fluctuations on the pulse shape, giving rise to the so-called *time walk*. A number of *time-pickoff methods* can be deployed to mitigate the walk effect. A common method is based on the *constant fraction triggering* (CFT), which consists in analysing the zero-crossing of a signal obtained by a linear combination of the pulse V, delayed by a fixed time $\tau_{\rm d}$, with $-k\,V$, where k is an attenuation coefficient. The triggering time $t_{\rm R}$ is defined as the time at which:

$$V(t_{\rm R} - \tau_{\rm D}) - k\,V(t_{\rm R}) = 0. \tag{2.135}$$

Since Eq. (2.135) is homogeneous in V, signals with the same time-shape, but different amplitude, will give the same triggering time $t_{\rm r}$, see Fig. 2.13. This method is however affected by a residual walk effect if the pulse shape differ from one event to another. In this case, one can try to reduce the delay time $\tau_{\rm D}$ as to trigger on the rising edge of the signals, where event-by-event changes are smaller, a technique known as *amplitude and risetime compensation* (ARC).

Solution

The time derivative of the signal is distributed in the range

$$\frac{dV}{dt} \in \left[\frac{V_{\rm min}}{T_{\rm S}}, \frac{V_{\rm max}}{T_{\rm S}}\right] = [0.05, 0.1]\,\frac{\mathrm{V}}{\mathrm{ns}}. \tag{2.136}$$

Signals with time derivatives at the edge of the interval of Eq. (2.136) will trigger the disciminator at times:

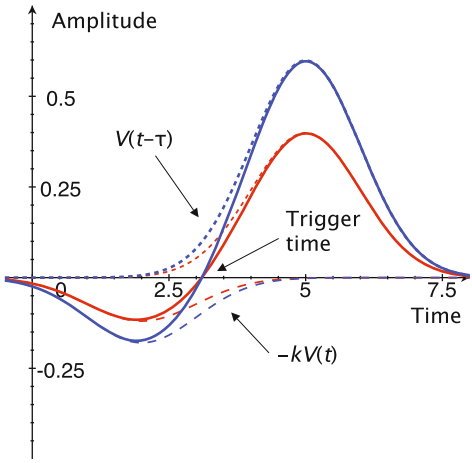

Fig. 2.13 Application of the CFT technique to a pair of Gaussian-like signals with different amplitude

$$t_{\min} = \frac{V_{\text{th}}}{V_{\max}/T_{\text{S}}} = \frac{0.4\,\text{V}}{0.1\,\text{V/ns}} = 4\,\text{ns}$$
$$t_{\max} = \frac{V_{\text{th}}}{V_{\min}/T_{\text{S}}} = \frac{0.4\,\text{V}}{0.05\,\text{V/ns}} = 8\,\text{ns} \tag{2.137}$$

The time walk Δt is therefore given by

$$\Delta t = t_{\max} - t_{\min} = 4\,\text{ns}. \tag{2.138}$$

A technique to eliminate the time walk is for example the constant fraction triggering, which is appropriate for this case since the signals feature the same rise-time.

Suggested Readings

Discriminators are briefly discussed in Sect. 14.0 of Ref. [1], while a few time-pickoff methods are described in Sect. 17.2 of the same reference. The reader is also addressed to Ref. [23] for application of discriminators in experiments.

Appendix 1

The computer program below illustrates the numerical evaluation of the information I_{ε_π} from Problem 2.28. The algorithm approximates the Rieman integral by the finite sum of rectangles:

$$\int dx\, f(x) \approx \sum_i f\left(\frac{x_{i+1} - x_i}{2}\right) \cdot \Delta x$$

The integral to be approximated is given by:

$$I_{\varepsilon_\pi} = \mathrm{E}\left[-\frac{\partial^2 f(x,\varepsilon_\pi)}{\partial^2 \varepsilon_\pi}\right] \equiv \int_{-\infty}^{+\infty} dt\ f(t,\varepsilon_\pi)\left[-\frac{\partial^2 \ln f(x,\varepsilon_\pi)}{\partial^2 \varepsilon_\pi}\right], \tag{2.139}$$

with:

$$\frac{\partial \ln f(x,\varepsilon_\pi)}{\partial \varepsilon_\pi} = \frac{\mathcal{N}(t;\ t_\pi,\sigma_t) - \mathcal{N}(t;\ t_K,\sigma_t)}{f(t,\varepsilon_\pi)} \tag{2.140}$$

$$\frac{\partial^2 \ln f(x,\varepsilon_\pi)}{\partial^2 \varepsilon_\pi} = -\frac{[\mathcal{N}(t;\ t_\pi,\sigma_t) - \mathcal{N}(t;\ t_K,\sigma_t)]^2}{f(t,\varepsilon_\pi)^2} \tag{2.141}$$

```
import math

# gaussian function
def gaus(x, m, s):
    return 1./math.sqrt(2*math.pi)/s * math.exp(-math.pow(x - m,2)/2/s/s)

m_pi = 6.68 $ TOF\index{Time of flight@Time-of-flight} for pi m_k
= 6.87 # TOF\index{Time of flight@Time-of-flight} for K sigma =
0.2 # std of TOF\index{Time of flight@Time-of-flight} measurement

def integrate(x_l=6.0, x_h=7.5, step=0.01, f_pi=0.5):
    integ = 0.0
    n_step = int((x_h-x_l)/step)
    for s in xrange( n_step ):
        t = x_l + (s+0.5)*step
        g_pi = gaus(t, m_pi, sigma)
        g_k = gaus(t, m_k, sigma)
        val = math.pow(g_pi - g_k, 2)/(f_pi*g_pi + (1. - f_pi) * g_k )
        integ += val*step
    return integ

##############################
for f_pi in [0.1, 0.3]:
    res = integrate(x_l=5., x_h=10, step=0.001, f_pi=f_pi)
    print f_pi"==>", res
```

References

1. W.R. Leo, *Techniques for Nuclear and Particle Physics Experiments*, 2nd edn. (Springer, Berlin, 1993)
2. C. Patrignani et al., (Particle Data Group). Chin. Phys. C **40**, 100001 (2016)
3. J.D. Jackson, *Classical Electrodynamics*, 3rd edn. (Wiley, New Jersey, 1999)
4. Yung-Su Tsai, Rev. Mod. Phys **46**, 815 (1974)
5. http://pdg.lbl.gov/2016/AtomicNuclearProperties

6. National Institute of Standards and Technology. XCOM: Photon Cross Sections Database (2012), http://nist.gov/pml/data/xcom/index.cfm
7. G.F. Knoll, *Radiation Detection and Measurement*, 4th edn. (Wiley, New Jersey, 2010)
8. F. Sauli, *Gaseous Radiation Detectors : Fundamentals and Applications* (Cambridge University, Cambridge, 2014)
9. A. Thompson et al., *X-ray Data Booklet*, LBNL/PUB-490 Rev.3 (2009)
10. D.E. Groom et al., Atomic Data Nucl. Data Tab. **78**, 183 (2001), https://doi.org/10.1006/adnd.2001.0861
11. A.A. Kochanov et al., Astropart. Phys. **30**, 219233 (2008), https://doi.org/10.1016/j.astropartphys.2008.09.008
12. ALEPH Collaboration Nucl, Instr. Methods A **360**, 481 (1995)
13. M. Peskin, D.V. Schroeder, *An introduction to Quantum Field Theory* (Advanced Book Program, Westview Press, 1995)
14. CMS Collaboration, Accepted by JINST, CMS-PRF-14-001, CERN-EP-2017-110, arXiv:1706.04965 (2017)
15. H. Primakoff, S. Rosen, Rep. Prog. Phys. **22**, 121–166 (1959)
16. *Stopping-power and range tables for electrons*, ICRU Report No. 37 (1984)
17. T. Tabarelli de Fatis, Eur. Phys. J. C **65**, 359 (2010), https://doi.org/10.1140/epjc/s10052-009-1207-8
18. K.S. Hirata et al., Phys. Rev. D **38**, 448–457 (1988), https://doi.org/10.1103/PhysRevD.38.448
19. R. Cahn, G. Goldhaber, *The Experimental Foundations of Particle Physics*, 2nd edn. (Cambridge University, Cambridge, 1989)
20. C.W. Fabjan, F. Gianotti, Rev. Mod. Phys. **75**, 1243–1286 (2003), https://doi.org/10.1103/RevModPhys.75.1243
21. L. Rossi et al., *Pixel Detectors* (Spinger, Berlin, 2006)
22. W. Blum, W. Riegler, L. Rolandi, *Particle Detection with Drift Chambers* (Springer, Berlin, 2008)
23. R. Frühwirth et al., *Data Analysis Techniques for High-Energy Physics*, 2nd edn. (Cambridge Press, Cambridge, 2000)
24. ATLAS Collaboration, JINST **11** P04008 (2016), https://doi.org/10.1088/1748-0221/11/04/P04008
25. C.M.S. Collaboration, JINST **8**, P04013 (2013), https://doi.org/10.1088/1748-0221/8/04/P04013
26. L. Rolandi, F. Ragusa, New J. Phys. **9**, 336 (2007), https://doi.org/10.1088/1367-2630/9/9/336

http://www.springer.com/978-3-319-70493-7

Selected Exercises in Particle and Nuclear Physics

Bianchini, L.

2018, XIV, 364 p. 56 illus., 40 illus. in color., Hardcover
ISBN: 978-3-319-70493-7